

30 **Abstract**

31

32 **The past two million years of eastern African climate evolution is poorly constrained**
33 **despite its assumed role in early human evolution¹⁻⁴. Rare paleoclimate records from**
34 **northeastern Africa suggest progressively drier conditions^{2,5} or a stable hydroclimate⁶.**
35 **In contrast, the only long records from Lake Malawi in tropical southeastern Africa**
36 **revealed a trend towards a progressively wetter climate over the last 1.3 Ma^{7,8}. The**
37 **climatic forcings that controlled these past hydrological changes are also a matter of**
38 **debate. Some studies suggest a dominant local insolation forcing on hydrological**
39 **changes⁹⁻¹¹ whereas others infer a potential influence of sea surface temperature (SST)**
40 **changes in the Indian Ocean^{8,12,13}. We present a multi-proxy reconstruction of**
41 **hydrological changes in the Limpopo River catchment of southeastern Africa (20-25°S),**
42 **in conjunction with a SST reconstruction in the southwestern Indian ocean over the past**
43 **2.14 Ma. Here, we show that hydroclimate in the region is controlled by an interplay**
44 **between low latitude insolation forcing (precession and eccentricity) and high latitude**
45 **ice volume changes. The long-term aridification in the Limpopo catchment between**
46 **around 1 Ma and 0.6 Ma is opposite to the hydroclimatic evolution at Lake Malawi and**
47 **seems related to equatorward contraction of the rainbelt in response to increased ice**
48 **volume at high latitudes. By impacting local terrestrial ecosystems, the observed**
49 **hydroclimate changes in southeastern Africa both in terms of long-term state and**
50 **marked precessional variability could have played a role in early hominin evolution,**
51 **particularly in the extinction of the species *Paranthropus robustus*.**

52

53

54 Subtropical southeastern Africa is a region of critical interest because it bears hominin fossils,
55 enabling a comparison between continental indicators of hominin evolution and nearby
56 marine records of past climate changes. Different modes of climate change have been
57 proposed as major factors influencing hominin speciation, adaptation, or extinction. Some
58 authors stress the impact of long-term trends toward aridity on hominin evolution^{1,2} whereas
59 others suggest a crucial role of short periods of extreme climatic variability in driving
60 hominin evolution^{3,4}.

61 *Paranthropus robustus* fossils have been found only in southeastern Africa and exclusively in
62 the Limpopo River catchment (sites of Cooper's D, Drimolen, Swartkrans, Sterkfontein,
63 Kromdraai B and Gondolin) (Fig. 1) from at least ~2 Ma to 0.9 Ma (Extended Data Table 1).
64 It is unclear whether climate stress could have played a role in its extinction.

65 To investigate the hydroclimatic context of the environment *P. robustus* lived in, we
66 reconstructed Quaternary hydrological cycle changes in subtropical southeastern Africa (20-
67 25°S) to determine the drivers of variability and to identify the long-term climate evolution of
68 this region. We used marine sediment core MD96-2048 (26°10'482''S, 34°01'148''E, 660 m
69 water depth) from offshore the Limpopo River (Fig. 1). The chronology of MD96-2048 is
70 established by tuning the $\delta^{18}\text{O}$ benthic foraminifera signal to the reference LR04 stack (Fig. 2)
71 (Methods), confirming that the core covers the last 2.14 Ma. We present a multi-proxy record
72 of hydrological changes in the Limpopo catchment together with a sea surface temperature
73 record of the southwestern Indian Ocean (Fig. 2).

74 Modern precipitation in the Limpopo catchment is dominated by austral summer rainfall
75 associated with the Intertropical Convergence Zone (ITCZ) extending southwards to 15-20°S
76 (Fig. 1). Changes in the hydrological cycle in the catchment are imprinted on Limpopo river
77 discharge. We observe large changes in terrestrial (Fe) versus marine (Ca) sedimentary

78 elemental ratios, indicating changes in terrestrial discharge by the Limpopo River, at orbital
79 and longer timescales (Fig. 2, Extended Data Fig. 1). Maxima in $\ln(\text{Fe}/\text{Ca})$ ratios are
80 associated with a more depleted stable hydrogen isotope composition of plant waxes ($\delta\text{D}_{\text{wax}}$)
81 (Fig. 2), which reflect the isotopic composition of precipitation and are indicative of higher
82 regional rainfall amount^{10,12,14} (Extended Data Fig. 2) (Methods). Maxima in $\ln(\text{Fe}/\text{Ca})$ ratios
83 are also associated with maxima in brGDGT concentrations (commonly found in soils and
84 attributed to Limpopo River runoff¹⁵) and more enriched plant wax $\delta^{13}\text{C}$. A previous study on
85 core MD96-2048 over the last 0.8 Ma interpreted shifts towards more depleted $\delta^{13}\text{C}_{\text{wax}}$ as
86 potentially reflecting more humid conditions¹⁶. However, $\delta^{13}\text{C}_{\text{wax}}$ is a proxy for the
87 contribution of waxes from C_3 versus C_4 plants to the sediments, which can be influenced by
88 many other factors than aridity/humidity. We attribute the enriched plant $\delta^{13}\text{C}_{\text{wax}}$ at times of
89 depleted $\delta\text{D}_{\text{wax}}$ values, increase $\ln(\text{Fe}/\text{Ca})$ and brGDGT concentration to stronger transport of
90 C_4 plant material from the upper Limpopo catchment in addition to the extension of riverine
91 swamps and floodplains harboring abundant C_4 sedges (Fig. 2, Extended Data Figs. 3 and 4).
92 The $\ln(\text{Fe}/\text{Ca})$ ratio has the highest temporal resolution (300 years on average) of the proxies
93 employed here. Statistical analyses indicate significant 19 and 23 kyr cycles (precession) and
94 100 kyr and 400 kyr cycles (eccentricity) but no significant 41 kyr cycle (obliquity) (Extended
95 Data Figs. 5). The dominance of eccentricity and precession cycles indicates a strong
96 influence of low-latitude insolation on hydrological changes in the Limpopo catchment.
97 Rainfall and precession maxima are in phase (i.e. maxima of local insolation in the southern
98 hemisphere) (Extended Data Figs. 3, 5).
99 Modern-day rainfall in the subtropical Limpopo region mostly depends on easterly waves and
100 low-pressure cells largely controlling summer rainfall (November to March, 72 % of the
101 rainfall in Pretoria; Extended Data Fig. 2), and on tropical-extratropical cloud bands and
102 associated thunderstorms¹⁷. The convective rains are usually associated with the ITCZ and
103 warm, humid easterly winds¹⁷. Numerical model experiments suggest southern summer
104 insolation forcing exerts a strong and positive effect on monsoon rainfall^{11,18}. During
105 precession maxima, higher southern hemisphere summer insolation causes higher
106 temperatures and lower surface pressure over the southern hemisphere, in particular over
107 land¹¹. The land/ocean temperature contrast results in stronger easterly moisture inflow onto
108 southeastern Africa. Increased rainfall results from increased convection over and increased
109 humidity transport onto southeastern Africa¹¹. Because eccentricity modulates precession
110 amplitudes, increased summer insolation associated with eccentricity increases the variability
111 in rainfall and fluvial discharge in the Limpopo catchment (Fig. 3).
112 In addition to this, it is thought that sea surface temperature anomalies in the Indian Ocean
113 have an influence on summer rainfall in the region¹⁹. To explore the potential relationship
114 between hydrological cycle changes and oceanic conditions, SSTs in the southwestern Indian
115 Ocean were reconstructed using two different methods (Methods, Extended Data Fig. 6).
116 There is a significant correlation between SST and orbital parameters at the 100 kyr cycle
117 (glacial-interglacial periodicity) and the 41 kyr cycle (obliquity) (Extended Data Fig. 5). The
118 results confirm a previous study revealing the absence of significant precessional variability
119 in the SST record over the last 800 kyr¹⁵. This suggests that orbital-scale precipitation changes
120 in southeastern Africa are more closely related to the land/ocean temperature contrast than to
121 SST changes.
122 Superimposed on the orbital-scale changes, our record displays a long-term trend towards
123 more arid conditions in southeastern Africa between ~ 1 Ma and ~ 0.6 Ma (Figs. 2, 3b-c). This
124 period corresponds to the Mid-Pleistocene Transition (MPT), which is marked by ice-sheet
125 expansion and global SST decrease²⁰ (Fig. 2). In terms of hydrological changes, the record
126 from Lake Malawi covering the last 1.3 Ma has been interpreted to show opposite changes to
127 those we observe for the Limpopo catchment. At Lake Malawi, the climate changed from a

128 predominantly arid environment between 1.3 and ~1 Ma to generally wetter conditions after
129 ~1 Ma^{7,8}. This opposing pattern in hydrological changes between the Limpopo catchment and
130 Lake Malawi suggests a gradual contraction of tropical rainfall from the Limpopo catchment
131 towards lower latitudes in response to the ice sheet expansion during the MPT. This rainfall
132 shift could be related to increased Antarctic ice volume during the MPT^{21,22}.

133 The long-term trend towards wetter conditions at Lake Malawi has been explained by a
134 progressively less positive Indian Ocean Dipole (IOD) since ~1 Ma. The IOD can enhance or
135 reduce the precessional variability in low-latitude hydroclimate by modifying the Walker
136 circulation over the Indian Ocean with a diverse response in eastern Africa²³. A progressively
137 less positive IOD would have generated wetter conditions in southern Africa and increased
138 the precession signal. Whilst the precessional signal increased over time at Limpopo, the
139 observed progressive increase in aridity is contrary to what would be expected with IOD
140 forcing alone (Fig. 3).

141 Based on our new records and comparison with Lake Malawi published records in eastern
142 Africa we propose that low latitude insolation forcing (precession and eccentricity) and high
143 latitude ice volume changes were the main driver of southeastern African hydroclimate over
144 the last 2 Ma with SST forcing playing a secondary role. Results also highlight a large
145 regional variability in southeastern African hydroclimate.

146 Hydrological cycle changes in southeastern Africa were likely one of the multiple factors
147 influencing the dispersal and evolution of human relatives^{2,4}. The more humid conditions
148 observed between ~2 Ma and 1.75 Ma associated with a maximum in eccentricity forcing
149 correspond to several occurrences of *P. robustus* (Fig. 3, Extended Data Table 1).
150 *Paranthropus robustus* is a species that was overall ecologically variable (eurytopic) but
151 multiple lines of evidence suggest that, from its earliest to its last occurrence, it preferred the
152 C₃ wooded or humid components of environments that were otherwise dominated by C₄ dry-
153 adapted plants. This preference for habitats dominated by C₃ plants, either in woodlands or in
154 humid environments, is well corroborated by the data gained from the paleoecological studies
155 of other contemporaneous animals, indicating large quantities of C₄ vegetation available, but
156 always with a more wooded component and a water source available nearby (Fig. 3B,
157 Extended Data Table 2, Methods)²⁴. Interestingly, this more humid period between ~2 Ma and
158 1.75 Ma is also characterized by the presence of *Australopithecus sediba* in the Limpopo
159 catchment (so far known only at the Malapa site)²⁵. Multiple lines of evidence similarly
160 suggest the latter lived in a wooded or humid habitat and had a diet dominated by C₃ plants
161 within an otherwise rather open environment dominated by C₄ plants²⁵.

162 Our new data raise the possibility that increasing long-term aridity associated to multi-
163 millennial-scale changes after 1 Ma driven by the MPT (Fig. 3b-d) could have diminished the
164 wooded and/or humid component of the habitat preferred by *P. robustus*. This is in
165 accordance with a trend towards more open and drier landscapes at Swartkrans (Fig. 3B,
166 Extended Data Table 2, Methods).

167 It has been proposed that extinctions of large mammals are mainly caused by abiotic
168 environmental changes²⁶. As a speculative but plausible scenario we propose that the
169 geographic ranges of species preferring wooded and humid habitats, including *P. robustus*,
170 would have contracted and expanded following the precessional (~21 kyr) dry and wet cycles.
171 During the multi-millennial dry periods, the range of populations of those species would have
172 contracted and often become fragmented. These isolated populations would have been
173 especially prone to local extinction through lack of sufficient suitable food, water, and
174 shelters, and related increased competition and predation. During multi-millennial wet periods
175 associated with precessional maxima, preferred woodland and humid habitats would have
176 expanded again. The surviving populations would have thrived again and expanded into their
177 previously occupied range, replacing locally extinct populations. The long-term trend to

178 increased aridity implies that the dry periods became more and more pronounced between 1
179 Ma and 0.6 Ma (Figs. 3b and 3d), increasing the likelihood for more numerous extinctions of
180 local populations, until the extinction of the last remaining population, and therefore of the
181 species²⁷. Given that the C₃ component of the vegetation preferred by *P. robustus* was never
182 dominant in the landscapes, even during humid periods, its populations would have been
183 especially prone to local extinction during dry periods.
184 Both the long-term aridification state and the extreme precessional hydroclimate variability
185 (Fig. 3) could thus have contributed to the extinction of *P. robustus*.

186
187
188
189
190
191
192
193
194
195
196
197
198
199
200
201
202
203
204
205
206
207
208
209
210
211
212
213
214
215
216
217
218
219
220
221
222
223
224
225
226
227

- 229 1. Vrba, E. S. Environment and evolution: alternative causes of the temporal distribution
230 of evolutionary events. *S. Afr. J. Sci.* **81**, 229–236 (1985).
- 231 2. deMenocal, P. B. Plio-Pleistocene African climate. *Science* **270**, 53–58 (1995).
- 232 3. Potts, R. Environmental hypotheses of hominin evolution. *Yearb. Phys. Anthropol.* **41**,
233 93–136 (1998).
- 234 4. Maslin, M. A. & Trauth, M. H. in *The First Humans: Origin and Early Evolution of*
235 *the Genus Homo* (eds Grine, F. E., Fleagle, J. G. & Leakey, R. E.) 151–158 (Springer,
236 2009).
- 237 5. Cerling, T. E. *et al.* Woody cover and hominin environments in the past 6 million
238 years. *Nature* **476**, 51–56 (2011).
- 239 6. Blumenthal, S. A. *et al.* Aridity and hominin environments. *Proc. Natl Acad. Sci. USA*
240 **114**, 7331–7336 (2017).
- 241 7. Lyons, R. P. *et al.* Continuous 1.3-million-year record of East African hydroclimate,
242 and implications for patterns of evolution and biodiversity. *Proc. Natl Acad. Sci. USA*
243 **112**, 15568–15573 (2015).
- 244 8. Johnson, T. C. *et al.* A progressively wetter climate in southern East Africa over the
245 past 1.3 million years. *Nature* **537**, 220–224 (2016).
- 246 9. Partridge, T. C., deMenocal, P. B., Lorentz, S. A., Paiker, M. J. & Vogel, J. C. Orbital
247 forcing of climate over South Africa: a 200,000-year rainfall record from the Pretoria
248 Saltpan. *Quat. Sci. Rev.* **16**, 1125–1133 (1997).
- 249 10. Schefuß, E., Kuhlmann, H., Mollenhauer, G., Prange, M. & Pätzold, J. Forcing of
250 south-east African wet phases during the last 17,000 years. *Nature* **480**, 509–512
251 (2011).
- 252 11. Simon, M. H. *et al.* Eastern South African hydroclimate over the past 270,000 years.
253 *Sci. Rep.* **5**, 18153 (2015).
- 254 12. Tierney, J. E. *et al.* Northern hemisphere controls on tropical southeast African
255 climate during the past 60,000 years. *Science* **322**, 252–255 (2008).
- 256 13. Dupont, L. M. *et al.* Glacial-interglacial vegetation dynamics in South Eastern Africa
257 coupled to sea surface temperature variations in the Western Indian Ocean. *Clim. Past*
258 **7**, 1209–1224 (2011).
- 259 14. Schefuß, E., Schouten, S. & Schneider, R. R. Climatic controls on central African
260 hydrology during the past 20,000 years. *Nature* **437**, 1003–1006 (2005).
- 261 15. Caley, T. *et al.* High-latitude obliquity as a dominant forcing in the Agulhas current
262 system. *Clim. Past* **7**, 1285–1296 (2011).
- 263 16. Castañeda, I. S. *et al.* Middle to Late Pleistocene vegetation and climate change in
264 subtropical southern East Africa. *Earth Planet. Sci. Lett.* **450**, 306–316 (2016).
- 265 17. Tyson, P. D. & Preston-Whyte, R. A. *The Weather and Climate of Southern Africa*
266 (Oxford University Press, 2000).
- 267 18. Kutzbach, J. E., Liu, X., Liu, Z. & Chen, G. Simulation of the evolutionary response
268 of global summer monsoons to orbital forcing over the past 280,000 years. *Clim. Dyn.*
269 **30**, 567–579 (2008).
- 270 19. Reason, C. J. C. Subtropical Indian Ocean SST dipole events and southern African
271 rainfall. *Geophys. Res. Lett.* **28**, 2225–2227 (2001).
- 272 20. McClymont, E. L., Sostdian, S. M., Rosell-Melé, A. & Rosenthal, Y. Pleistocene sea-
273 surface temperature evolution: early cooling, delayed glacial intensification, and
274 implications for the mid-Pleistocene climate transition. *Earth Sci. Rev.* **123**, 173–193
275 (2013).
- 276 21. Elderfield, H. *et al.* Evolution of ocean temperature and ice volume through the mid-
277 Pleistocene climate transition. *Science* **337**, 704–709 (2012).

- 278 22. Pollard, D. & DeConto, R. M. Modelling West Antarctic ice sheet growth and collapse
279 through the past five million years. *Nature* **458**, 329–332 (2009).
- 280 23. Tierney, J. E., Smerdon, J. E., Anchukaitis, K. J. & Seager, R. Multidecadal variability
281 in East African hydroclimate controlled by the Indian Ocean. *Nature* **493**, 389–392
282 (2013).
- 283 24. Balter, V., Braga, J., Télouk, P. & Thackeray, J. F. Evidence for dietary change but
284 not landscape use in South African early hominins. *Nature* **489**, 558–560 (2012).
- 285 25. Henry, A. G. *et al.* The diet of *Australopithecus sediba*. *Nature* **487**, 90–93 (2012).
- 286 26. Žliobaitė, I., Fortelius, M., & Stenseth, N. C. Reconciling taxon senescence with the
287 Red Queen’s hypothesis. *Nature* **552**, 92–95 (2017).
- 288 27. Foley, R. in *African Biogeography, Climate Change, and Human Evolution* (eds
289 Bromage, T.G. & Schrenk, F.) 328–348 (Oxford University Press, 1999).
- 290 28. Xie, P. & Arkin, P. A. Global precipitation: a 17-year monthly analysis based on
291 gauge observations, satellite estimates and numerical model outputs. *Bull. Am.*
292 *Meteorol. Soc.* **78**, 2539–2558 (1997).
- 293 29. Locarnini, R. A. *et al.* *World Ocean Atlas 2009. Volume 1: Temperature.* (NOAA
294 Atlas NESDIS 68, U. S. Government Printing Office, 2010).
- 295 30. Still, C. J. & Powell, R. L. in *Isoscapes: Understanding Movement, Pattern, and*
296 *Process on Earth through Isotope Mapping* (eds West, J. B., Bowen, G. J., Dawson, T.
297 E. & Tu, K. P.) 179–194 (Springer, 2010).
- 298 31. Laskar, J. *et al.* A long-term numerical solution for the insolation quantities of the
299 Earth. *Astron. Astrophys.* **428**, 261–285 (2004).

300

301

302

303

304

305

306

307

308

309

310

311

312

313

314

315

316

317 **Supplementary Information** is linked to the online version of the paper at
318 www.nature.com/nature.

319 **Acknowledgements:** T.C. is supported by CNRS-INSU. Funding from LEFE-IMAGO CNRS
320 INSU project SeaSalt is acknowledged. T.C. was partly supported by the “Laboratoire
321 d’Excellence” LabexMER (ANR-10-LABX-19) and co-funded by a grant from the French
322 government under the program “Investissements d’Avenir”, and by a grant from the Regional
323 Council of Brittany (SAD programme). J.A.C. acknowledges funding from the ERC-project
324 “STEEPCLim”. E.S. and L.D. acknowledge funding through the DFG-Research
325 Center/Cluster of Excellence “The Ocean in the Earth System” at MARUM – Center for
326 Environmental Sciences. A.S. acknowledges funding through the LaScArBx, a programme
327 supported by the Agence Nationale pour la Recherche (ANR-10-LABX-52). Core MD96-
328 2048 was collected during the MOZAPHARE cruise of the RV Marion Dufresne, supported
329 by the French agencies Ministère de l’Education Nationale de la Recherche et de la
330 Technologie, Centre National de la Recherche Scientifique (CNRS), and Institut Paul Emile
331 Victor (IPEV).

332 **Author contributions:** T.C. designed the study. T.C., T.E., M.W., and P-Y.G performed the
333 Mg/Ca measurements. L.R. analysed the foraminifera assemblages and T.C. and F.E.
334 analysed the results and performed the transfer function. T.C., T.E., B.M. and K.C performed
335 the $\delta^{18}\text{O}$ analyses on foraminifera. T.C., J.G., P.M. and I.B performed the XRF measurements
336 and F.J.J-E and C.G-C. conducted the statistical analyses on XRF. J.A.C. and E.S. performed
337 plant-wax δD and $\delta^{13}\text{C}$ analyses. L.D. performed the pollen analysis. A.S. and T.C. produced
338 the synthesis on the ecology and environments of South African hominins and conducted the
339 comparisons to the marine record. T.C. and D.M.R. performed and analysed the iLOVECLIM
340 model results. T.C. analysed the results and all authors participated in the interpretation. T.C.
341 wrote the manuscript with contributions from all authors.

342 **Author Information:** Reprints and permissions information is available at
343 www.nature.com/reprints. The authors declare no competing financial interests.
344 Correspondence and requests for materials should be addressed to T.C.

345

346

347

348

349

350

351

352

353

354

355

356 **Figure legends**

357

358 **Figure 1: Modern climatology over southern Africa and vegetation types in the Limpopo**
359 **catchment.** a) Averaged precipitation rates for January²⁸ and annual SST over the Indian
360 Ocean²⁹. Black arrows represent the atmospheric circulation over southern Africa during
361 austral summer. The Intertropical Convergence Zone (ITCZ) and the Congo Air Boundary
362 (CAB) are indicated. b) Modelled relative C₄ plant abundance in the Limpopo catchment³⁰
363 with indications of topography and bathymetry. Location of core MD96-2048, the Lake
364 Malawi records, the main sites of hominin finds for *Paranthropus robustus* (sites of Cooper's
365 D, Drimolen, Swartkrans, Sterkfontein, Kromdraai B and Gondolin) and *Australopithecus*
366 *sediba* (Malapa) (Extended Data Table 1) and the Pretoria GNIP station are indicated.

367 **Figure 2: Hydrological changes in the Limpopo catchment compared to sea surface**
368 **temperatures of the southwestern Indian Ocean over the last 2.14 Ma.** a) δD of the *n*-C₃₁
369 alkane of plant waxes. Mean analytical uncertainty of 3 ‰ is indicated. b) $\delta^{13}C$ of the *n*-C₃₁
370 alkane of plant waxes (from Castaneda et al.¹⁶ in light green and this study in dark green).
371 Mean analytical uncertainties of 0.2 ‰ and 0.4 ‰¹⁶ are indicated. c) Pollen percentages of
372 Cyperaceae (data of the last 342 kyr from Dupont et al.¹³). Error bars represent 95 %
373 confidence intervals. d) $\ln(Fe/Ca)$ XRF ratios. Arrow indicates the long-term trend discussed
374 in the text. Grey frames represent events of hydrological cycle intensification. e) Principal
375 component of the SST records (Methods). f) $\delta^{18}O$ of benthic foraminifera compared to the
376 reference LR04 curve (data of the last 790 kyr from Caley et al.¹⁵) (Methods). The Mid
377 Pleistocene Transition (MPT) period is indicated.

378 **Figure 3: Forcings on the hydrological cycle changes in the Limpopo catchment and**
379 **relationship with hominin evolution over the last 2.14 Ma.** A. a) Eccentricity and
380 precession index³¹. b) $\ln(Fe/Ca)$ XRF ratios as a proxy of hydrological changes in the
381 Limpopo catchment. Red curve denotes a polynomial fit (9th degree). The MPT and the
382 associated ice-sheet expansion is indicated (orange shading)^{20,21}. Grey shading indicates
383 wetter conditions in the Limpopo catchment associated with higher eccentricity. c) Cusum of
384 $\ln(Fe/Ca)$ showing deviation from the mean as indicator of hydrological variability in the
385 Limpopo catchment (Methods) (red curves correspond to dry periods, yellow curves to drying
386 periods, dark blue curves to wet periods and light blue curves to humidification periods). d)
387 Precession component of the $\ln(Fe/Ca)$ ratios obtained by Gaussian filtering. e) Estimated
388 ages for the main sites that yielded remains of the hominin *Paranthropus robustus* (Cooper's
389 D, Drimolen, Swartkrans and Gondolin) and *Australopithecus sediba* (Malapa) (Extended
390 Data Table 1). B. Enamel $\delta^{13}C$ (‰ V-PDB) of hominins and contemporaneous herbivores at
391 Swartkrans (Extended Data Table 2). Triangles indicate raw data points. The boxplots
392 correspond to the median (horizontal line), the interquartile range (box), and the full range of
393 data (vertical whiskers). Sample sizes are indicated in parentheses. Dash lines highlight the
394 thresholds used to estimate the percentage of C₃ plants-derived foods in the diets.

395

396 **Methods:**

397 **XRF measurements:** Element intensities were measured using a XRF-Avaatech core scanner
398 at EPOC, Bordeaux. Before analysis, the sediment surface was flattened and covered with
399 Ultralene film. The core sections were scanned at a 0.5 cm resolution at two different levels of
400 energy (10 and 30 keV).

401 In order to easily identify periods in XRF $\ln(\text{Fe}/\text{Ca})$ record, we computed the cumulative sum
402 (Cusum) of the deviations from the mean:

403
$$\text{Cusum} = \text{sum}(\ln(\text{Fe}/\text{Ca}) - \text{mean}(\ln(\text{Fe}/\text{Ca})))$$

404 The Cusum method was developed for industrial control to detect changes in sequential
405 production³². More recently, the Cusum has been extensively applied in biological
406 oceanography (e.g. García-Comas et al.³³) following Ibanez et al.³⁴. The Cusum shows
407 periods (i.e., linear sequences) and their value in respect to the long-term average: a positive
408 slope shows a period of values greater than the long-term average, while a negative slope
409 shows a period of values smaller than the long-term average. The steepness of the slope
410 reflects how different a period is from the long-term average. Furthermore, changes in the
411 tendency (i.e., sequential periodical changes in the slope) reflect periodical changes from a set
412 of conditions to another (e.g., a change from a positive slope to a flat slope in the XRF
413 $\ln(\text{Fe}/\text{Ca})$ record reflects a change from a humid period to a drier period). In the case of the 1
414 Ma to 0.6 Ma interval, this corresponds to a period of aridification because it is more arid than
415 the previous period between 1.2 Ma to 1 Ma (i.e., there is a change of slope from steep
416 positive to slightly negative). In addition, the period between 1 Ma to 0.6 Ma is very variable
417 because the slope is not straight but noisy. The Cusum can be found under the function name
418 `local.trend`, in the R package: `Pastecs: Package of Analysis of Space-Time Ecological Series`.

419 **Plant-wax δD and $\delta^{13}\text{C}$:** Plant-wax analyses were carried out at MARUM, University of
420 Bremen. Samples were oven dried at 40°C, homogenized and squalane was added as internal
421 standard before extraction. Lipids were extracted with a DIONEX Accelerated Solvent
422 Extractor using a 9:1 mixture of dichloromethane to methanol at 100°C and 1000 psi for five
423 minutes, repeated three times. The saturated hydrocarbon fraction was obtained by elution of
424 the dried lipid extract over a silica column with hexane and subsequent elution over AgNO_3 -
425 coated silica to remove unsaturated hydrocarbons.

426 Compound-specific stable carbon isotope ($\delta^{13}\text{C}$) analyses were carried out using a
427 ThermoFisher Scientific Trace GC Ultra coupled to a Finnigan MAT 252 isotope ratio
428 monitoring mass spectrometer via a combustion interface operated at 1000°C. Isotope values
429 were calibrated against external CO_2 reference gas and are reported as permille (‰) against
430 the Vienna PeeDee Belemnite (VPDB) standard. Samples were run at least in duplicate. The
431 internal standards yielded a precision of ≤ 0.3 ‰. Repeated analysis of an external *n*-alkane
432 standard between samples yielded a root-mean-squared accuracy of 0.1 ‰ and a standard
433 deviation of on average 0.2 ‰.

434 When possible, given the high amount of lipids necessary, compound-specific stable
435 hydrogen isotope (δD) compositions were measured using a ThermoFisher Scientific Trace
436 GC coupled via a pyrolysis reactor operated at 1420°C to a ThermoFisher MAT 253 isotope
437 ratio mass spectrometer. δD values were calibrated against external H_2 reference gas, the 3H+
438 factor was monitored daily (values vary between 6.7 and 6.9); δD values are reported in
439 permille (‰) versus the Vienna Standard of Mean Ocean Water (VSMOW) standard. The
440 internal standards yielded a precision of 2 ‰ on average. Repeated analysis of an external *n*-

441 alkane standard between samples yielded a root-mean-squared accuracy of <1 % and a
442 standard deviation of on average 3 ‰.
443 Results of a method to adjust the δD_{wax} record for vegetation and ice-volume changes is
444 proposed in Extended Data Fig. 4.

445

446 **Pollen preparation:** Samples of 1.5 to 8.5 ml were prepared at MARUM. The volume was
447 measured using water displacement. Samples were decalcified with diluted HCl (~12 %) and
448 treated with HF (~40 %) to remove silicates. Samples were sieved over a screen to remove
449 particles smaller than 10–12 μm . When necessary the sample was decanted to remove
450 remaining silt. Samples were stored in water, mounted in glycerol, and microscopically
451 examined (magnification 400 and 1000x) for pollen and spores. Cyperaceae (sedges) pollen
452 percentages were calculated based on the total number of pollen and spores ranging from 53
453 to 365 and 95 % confidence intervals were calculated after Maher³⁵.

454

455 **$\delta^{18}\text{O}$ analyses on foraminifera:** Specimens of benthic *Planulina wuellerstorfi* foraminifera
456 were picked from the 250-315 μm size fraction. Analyses were carried out by a coupled
457 system Multiprep-Optima of Micromass© at EPOC. The automated preparation system
458 (Multiprep) transforms carbonate samples into CO_2 gas by treatment with orthophosphoric
459 acid at a constant temperature of 75°C. The CO_2 gas samples were then analysed by isotope
460 mass spectrometry (Optima) in comparison with a calibrated reference gas to determine the
461 isotopic ratio $^{18}\text{O}/^{16}\text{O}$ of the sample. For all stable oxygen isotope measurements a working
462 standard (Burgbrohl CO_2 gas) was used, which was calibrated against the Vienna Pee Dee
463 Belemnite (VPDB) standard by using the NBS 19 standard. Analytical standard deviation is
464 about 0.05 ‰ ($\pm 1\sigma$).

465 The chronology of the core was established by tuning the $\delta^{18}\text{O}$ benthic foraminifera signal to
466 the reference LR04 stack³⁶ with the AnalySeries software³⁷ and yielded a correlation
467 coefficient of $R = 0.8$ for the last 2.14 Ma. The core is ca. 36 meter long and the
468 sedimentation rate has a mean value of 2 cm/kyr ($\sigma = 0.91$) and is relatively constant.

469

470 **SSTs reconstruction:** *Globigerinoides ruber s. s.* were picked within the 250-315 μm size
471 fraction for trace element analyses. Shells were cleaned at EPOC to eliminate contamination
472 by clays and organic matter based on the procedure of Barker et al.³⁸. An Agilent Inductively
473 Coupled Plasma Optical Emission Spectrometer (ICP-OES) was used for magnesium and
474 calcium analyses following the procedure established by De Villiers et al.³⁹. Reproducibility
475 obtained from *G. ruber s. s.* on 80 samples from the complete core was better than 6 % ($\pm 1\sigma$,
476 pooled RSD). All new analyses for this study ($n = 217$) were performed at EPOC. Measured
477 Mg/Ca ratios were converted into temperature values applying the equation established by
478 Anand et al.⁴⁰ yielding a precision of 1.2°C.

479 Total assemblages of planktonic foraminifera were analyzed at EPOC using an Olympus
480 SZH10 binocular microscope following the taxonomy of Hemleben et al.⁴¹ and Kennett et
481 al.⁴². About 300 specimens were counted in each level after splitting with an Otto
482 microsplitter. Relative abundances of species were used to perform quantification of SST after
483 an ecological transfer function⁴³ developed at EPOC. The method used here is based on the
484 Modern Analogue Techniques (MAT)⁴⁴ running under the R software, using a script first
485 developed for dinocyst transfer functions by Guiot and Brewer. The modern database used is
486 composed of 367 core tops and derived from the ones covering the southern Indian Ocean⁴⁵ in
487 the MARGO project. Calculations of past hydrological parameters rely on a weighted average
488 of SST values from the best five modern analogues, with a maximum weight given for the

489 closest analogue in terms of statistical distance, i.e., dissimilarity minimum^{43,46}. This method
490 permits the reconstruction of annual SST with a precision of 0.8°C (Extended Data Fig. 7).

491 As each proxy has some uncertainty related to the calibration, non-temperature influences and
492 lateral advection¹⁵, we applied Empirical Orthogonal Function (EOF) analysis⁴⁷ on the two
493 SST records over the last 2.14 Ma (Extended Data Fig. 6). The first Principal Component
494 (PC1) explains 74 % of the total variance for the Mg/Ca and foraminifera transfer function
495 records over the last 2.14 Ma. Correlation between SST proxies and PC1 over the last 2.14
496 Ma is R= 0.71.

497 **Climate modeling:** To investigate the control on the past δD composition of precipitation in
498 the Limpopo catchment we analyzed the results of a transient run with the intermediate
499 complexity isotope-enabled climate model iLOVECLIM⁴⁸⁻⁵⁰ over the last 150 kyr⁵¹. The
500 atmospheric part of the coupled climate model was run at T21 spatial resolution (~5.65°
501 lat,lon) and used accelerated forcing (irradiance, GHGs and ice sheets were updated with an
502 acceleration factor 10)⁵¹. Intermediate complexity models experiences some weaknesses
503 caused by the spatial resolution and simplified convective physics but have the advantage to
504 compute efficiently. iLOVECLIM was previously successfully applied in the Asian monsoon
505 region⁵¹ and in the West African monsoon region⁵² to investigate past monsoonal
506 precipitation changes and their links with changes in the isotopic composition of precipitation.
507 For the current study, analysis of its present-day performance for the region together with
508 results over the past 150 kyr are shown in Extended Data Figure 2.

509 **Ecology and environment of the hominins *Paranthropus robustus* and *Australopithecus***
510 ***sediba* in the Limpopo catchment:** Building on previous research (e.g., see recent
511 syntheses^{53,54}), we produced a short synthesis of multiple lines of evidence to reconstruct the
512 ecology and environmental context of the southern African robust australopith *Paranthropus*
513 *robustus*. We also discuss briefly *Australopithecus sediba*. Much literature has been devoted
514 to the ecology of the robust australopiths, and particularly the ecological differences between
515 *P. robustus* and *P. boisei*, another species found in eastern Africa. Given the geographic scope
516 of our paper centered on South Africa, we here focus our review mostly on *P. robustus*. The
517 reader should note that it is still a matter of debate whether the robust australopiths, namely *P.*
518 *robustus*, *P. boisei*, and *P. aethiopicus* (the likely ancestor of *P. boisei*, also found in eastern
519 Africa) are closely related to each other forming a monophyletic genus, or the robust adaptive
520 traits evolved independently by convergence/parallelism in eastern Africa and southern
521 Africa, making the *Paranthropus* genus diphyletic^{54,55}. Authors supporting the diphyletic
522 hypothesis tend to classify the robust australopiths in the genus *Australopithecus*. Until the
523 issue is settled, we use here the genus name *Paranthropus* as a convenient taxonomic label of
524 a grade grouping those three taxa that share similar robust adaptive features that differ from
525 the other more gracile genera *Australopithecus* and *Homo*.

526 **Craniomandibular and dental morphology:** species of *Paranthropus* are characterized by a
527 suite of peculiar craniomandibular and dental morphological characters: reduced incisors and
528 canines, molarized premolars, enlarged molars, thick enamel, enlarged insertion areas for
529 temporal muscles, robust mandibular corpus⁵⁶. This suite of robust morphological traits has
530 been frequently interpreted as potential adaptations to diets including hard foods (e.g.,^{57,58}).
531 This interpretation is partly supported in *P. robustus* by the dental microwear data that
532 indicate occasional consumption of hard objects (see below). Other authors suggested that

533 those characters reflect the ability of *Paranthropus* for prolonged chewing of tough plant
534 matter^{59,60}. This alternative interpretation is supported by the dental microwear and stable
535 carbon isotopic data in *P. boisei*^{61,62}. This interpretation could apply to *P. robustus* as well,
536 even though this species was likely feeding on different kinds of plants (C₄ herbaceous plants
537 in *P. boisei* versus various C₃ and C₄ plants in *P. robustus*, see below).

538 Potential modern analogs of herbivorous mammals that evolved from omnivorous ancestors
539 with thick enamel and bunodont molars include the giant panda *Ailuropoda melanoleuca* and
540 the red panda *Ailurus fulgens*, both highly specialized independently on a diet of tough
541 bamboo leaves requiring prolonged chewing and numerous repeated chewing cycles
542 (e.g.,^{63,64}). Both examples illustrate phylogenetic inertia, with evolution tinkering preexistent
543 morphologies, which limits the range of possible adaptive traits in response to functional
544 selective pressure and results in seemingly suboptimal morphologies for the realized diet. A
545 similar argument was made for *Paranthropus*^{53,65}. Therefore, contrary to herbivorous
546 ungulates that evolved long shearing crests and a more lateral mastication to reduce plant
547 matter into small digestible fragments, the giant panda, the red panda, and *Paranthropus*
548 evolved alternative solutions combining a thick enamel and increased dental surface with
549 prolonged use of high masticatory forces.

550 It was also suggested that an increased dental occlusal surface in mammals could be an
551 adaptive trait for feeding on small bites of small sized food items⁶⁶ by increasing the chance
552 of efficiently masticating the food items with a reduced number of chewing cycles, and
553 limiting the wear induced by a strong increased attrition (tooth to tooth contact) in addition to
554 the wear induced by abrasion (tooth to food contact). Similar adaptive traits, most notably
555 enlarged surfaces of third molars, evolved independently multiple times in African
556 herbivorous suids⁶⁷.

557 Compared to *Paranthropus*, the craniomandibular and dental morphology of *A. sediba* is
558 more gracile and more similar to the one found in older species of *Australopithecus* and
559 younger species of *Homo*. It was recently argued that the morphology of the cranium was
560 unsuited for feeding on hard objects⁶⁸ while that of the mandible was⁶⁹.

561 **Postcranial morphology:** very little is known about the postcranial morphology of *P.*
562 *robustus* but most studies indicate retention of traits adaptive to arboreal climbing (e.g.,^{70,71}).
563 Hand morphology suggests an ability to perform precision gripping during tool making and
564 using activities⁷². Numerous bone tools are found in Swartkrans Member 3 and Drimolen,
565 sites that yielded numerous specimens of *P. robustus*. Microscopic and macroscopic wear
566 analyses as well as experimental data suggest that those tools were used for digging into
567 termite mounds⁷³⁻⁷⁵. The scarcity of *Homo* remains compared to those of *P. robustus* in sites
568 bearing the bone tools suggests that the latter species is the most likely tool maker and user⁷³⁻
569 ⁷⁵. *Australopithecus sediba* is known by two partial skeletons that provide numerous
570 information on its postcranial morphology. Its upper limbs and shoulders retain numerous
571 adaptive traits for climbing and suspensory behaviors^{76,77}.

572 **Microstructure and biomechanics of enamel:** a study of the dental microstructure of *P.*
573 *robustus* indicates that its enamel was decussated (contrary to *P. boisei*⁷⁸), which is assumed
574 to reflect a capacity to withstand strong and/or prolonged biomechanic constraints during
575 mastication. Other mammals feeding on hard objects, such as hyaenids⁷⁹, and mammals
576 feeding on tough vegetation, such as many ungulates, also display decussated enamel⁸⁰.

577 In addition, an experimental study on the behavior of enamel under various biomechanic
578 constraints suggests that thick enamel could be an adaptive trait to deal with foods either hard
579 or tough, laden with particulates, potentially including both grit and phytoliths⁸¹. A recent
580 study observed a low frequency of enamel chipping in *P. robustus*, concluding that it was not
581 adapted to eating hard foods⁸², but rather tough vegetation. This interpretation is at odds with
582 the dental microwear data that indicate at least some consumption of hard objects (see below).
583 Alternatively, we argue that it is equally plausible that this low frequency of chipping is
584 related to the specialized decussated microstructure that reinforces the tooth enamel of *P.*
585 *robustus* at a microscopic scale, making its teeth less prone to chipping and therefore more
586 durable when consuming hard foods, as well as tough foods.

587 **Enamel biogeochemistry:** numerous data are available regarding the stable carbon and
588 oxygen isotopic compositions (expressed as $\delta^{13}\text{C}$ and $\delta^{18}\text{O}$, respectively), and the major
589 elements (Sr, Ba, Ca) of the enamel of *P. robustus*, of other hominins, as well as other
590 contemporaneous animals. The stable carbon isotope ratios enable to quantify the proportions
591 of food items deriving, directly or indirectly (through one or several trophic levels), from C_3
592 plants (mostly woody vegetation, but also sedges in humid environments) and C_4 plants
593 (mostly grass and sedges, but also shrubs of the Amaranthaceae/Chenopodiaceae family). The
594 $\delta^{13}\text{C}$ values of the enamel of *P. robustus* indicate a diet dominated by C_3 plants-derived foods,
595 with a significant proportion (ca. 35-40 %) of C_4 plants-derived foods (Fig. 3B and Extended
596 Data Table 2). Much efforts were dedicated to identify the food items that compose this
597 significant C_4 component in the diet of *P. robustus*⁸³⁻⁸⁶. Most likely C_4 plants-derived food
598 items include grass leaves and roots, insects such as grasshoppers and termites, small
599 vertebrates consuming C_4 plants or C_4 plants-eating invertebrates (birds, lizards, rodents,
600 small ungulates). Sedges are also considered a likely source of C_4 resources, notably through
601 the consumption of their Underground Storage Organs (USOs)^{87,88}. Sponheimer et al.⁸⁴
602 however argued that C_4 sedges were rather scattered in South African riverine settings and
603 that not many of them produced large palatable USOs. They therefore considered C_4 sedges as
604 a minor food resource for hominins. However, they only studied the sedges from four riverine
605 sites located in the Kruger National Park and it remains unknown whether their conclusions
606 would hold out for the whole Limpopo catchment and larger scales.

607 More important in our opinion is the fact that the diet of *P. robustus* was dominated by C_3
608 plants-derived food resources. The latter could include any parts (leaves, stems, fruits, nuts,
609 USOs) of C_3 plants (mostly trees, shrubs, bushes in wooded environments but also abundant
610 sedges in humid environments). Data on the enamel $\delta^{13}\text{C}$ values of *A. sediba* are very few (n
611 = 2) but both specimens display low values (-12.1 ‰ and -12.2 ‰) that indicate a diet
612 dominated by C_3 plants-derived food resources²⁵.

613 Stable oxygen ratios of enamel are related to multiple factors, including behavior, ecology,
614 diet, physiology, and climate⁸⁹. Levin et al.⁹⁰ classified mammals into Evaporation Sensitive
615 (ES) taxa and Evaporation Insensitive (EI) taxa. The $\delta^{18}\text{O}$ values in ES taxa increase with
616 aridity. ES taxa do not drink much and get most of the required water from the plants they
617 consume. Conversely, $\delta^{18}\text{O}$ values of EI taxa track the $\delta^{18}\text{O}$ values of surface water that they
618 drink abundantly and frequently^{90,91}. Although hominins were not included into this
619 classification scheme, they are likely water-dependent since all large primates need to drink a
620 lot of water every day. Hominins generally display relatively low $\delta^{18}\text{O}$ values on average
621 compared to the rest of the faunas^{62,92}, suggesting a high water dependence or consumption of

622 plants containing little evaporated water. Those data support the preference of *P. robustus* for
623 wooded and/or humid environments.

624 Intra-tooth variations of $\delta^{13}\text{C}$ and $\delta^{18}\text{O}$ also inform us about the intra-annual and inter-annual
625 variations in ecology. Such intra-tooth $\delta^{13}\text{C}$ and $\delta^{18}\text{O}$ profiles were measured using laser
626 ablation on four teeth of *P. robustus* from Swartkrans Member 1⁸³. The mean values of the
627 $\delta^{13}\text{C}$ profiles are similar to those of other *P. robustus* sampled previously, and they also reveal
628 significant intra-tooth variations with ranges varying from 2 ‰ to 5 ‰ over periods
629 representing approximately one or two years (inferred from the number of perikymata).
630 Significant positive correlations between the $\delta^{13}\text{C}$ and $\delta^{18}\text{O}$ in three out of four specimens of
631 *P. robustus* also indicate that they consumed relatively more C_4 plants-derived foods during
632 the dry seasons than during the wet seasons⁸³. This could suggest an opportunistic sampling of
633 the environment, with a relative consumption of C_3/C_4 plants-derived foods depending partly
634 on seasonal or inter-annual climatic differences. Those data are also congruent with the
635 identification of *P. robustus* as an EI taxon and are similar to the pattern observed in some
636 extant EI herbivorous ungulates (e.g., strong positive correlations of $\delta^{13}\text{C}$ and $\delta^{18}\text{O}$ profiles in
637 an extant common hippopotamus *Hippopotamus amphibius*⁹³).

638 Investigations of trace elements preserved in the enamel of *P. robustus* also revealed
639 interesting patterns^{24,94}. *Paranthropus robustus* is characterized by relatively high Sr/Ca
640 ratios, lower than in grazing ungulates, and a bit higher than in carnivores, browsing
641 ungulates, and omnivorous cercopithecoid monkeys. Interestingly, *A. africanus* is characterized
642 by even higher Sr/Ca ratios. Both hominins, but especially *A. africanus*, display low Ba/Ca
643 ratios. Altogether, those data indicate a likely low proportion of animal matter in their diets.
644 More interestingly, the only extant animals combining a high Sr/Ca ratio and a low Ba/Ca are
645 the mole rat (*Cryptomys hottentotus*), and to a lesser extent, the common warthog
646 (*Phacochoerus africanus*). Both species consume large amounts of grass roots. This could
647 indicate that grass root consumption was a significant aspect of *P. robustus* diet, explaining
648 part of the C_4 component of the diet. However, the Sr/Ca and the Ba/Ca ratios of *A. africanus*
649 and *P. robustus* are not as extreme as those found in the mole rat and the common warthog,
650 suggesting that the consumption of grass roots was likely not as important as in those two
651 species. As highlighted by Sponheimer et al.⁹⁴ one must however stress that the use of major
652 elements concentrations in enamel as an indication of the diet of extant and extinct animals
653 still necessitate further studies. Balter et al.²⁴ observed Sr/Ca and Ba/Ca ratios for *P. robustus*
654 that are intermediate between those of *A. africanus* and early *Homo*, and similar to those of
655 browsers. They argue the diet of *P. robustus* was dominated by woody plants.

656 **Dental microwear:** investigations of dental microwear also provided useful information to
657 reconstruct the diet of *P. robustus*^{61,95-97}. Dental microwear mostly results from a combination
658 of abrasion (food to tooth contact) and attrition (tooth to tooth contact), both resulting in
659 various microscopic scars left at the surface of the enamel facets. Among hominins,
660 specimens of *P. robustus* are characterized by unique microwear textures that display strongly
661 variable complexities, ranging from low to very high values, and low anisotropies. This
662 pattern, originally observed on a few specimens, was later confirmed by a large-scale study of
663 dental microwear in *P. robustus*, including numerous specimens from various sites⁹⁸.
664 Similarities in dental microwear textures were noted between *P. robustus* and some specimens
665 of several extant primates that are known to consume hard objects such as nuts and seeds
666 (gray-cheeked mangabeys *Lophocebus albigena*, brown capuchins *Cebus apella*), indicating

667 at least some consumption of hard objects by *P. robustus*. Dental microwear data available for
668 *A. sediba*, although based on two specimens only, also show high complexities, suggesting a
669 potential consumption of hard objects²⁵.

670 **Stable carbon isotopes of contemporary mammals:** compiled data of $\delta^{13}\text{C}$ values for
671 herbivorous mammals that were contemporary and sympatric with *P. robustus* indicate
672 habitats encompassing a mix of C_3 and C_4 plants, suggesting a mix of woodlands and
673 grasslands in all sites that were sampled (data for Swartkrans members 1, 2, and 3^{83,84,99,100};
674 Cooper's D¹⁰¹; Gondolin¹⁰²; Fig.3B and Extended Data Table 2). The enamel $\delta^{13}\text{C}$ values of
675 herbivorous mammals in all *P. robustus*-bearing sites where sufficient data are available
676 display a bimodal distribution (Extended Data Table 2): the main mode indicates that the
677 habitat was dominated by herbivorous mammals consuming mostly C_4 plants, while the
678 secondary mode indicates that a significant portion of the remaining herbivorous mammals
679 consumed C_3 plants. Mammals displaying a strong C_4 signal in their enamel likely consumed
680 herbaceous plants, including mostly dry-adapted C_4 grasses in open habitats and possibly C_4
681 sedges in humid habitats. They are usually classified as grazers. Conversely, mammals
682 displaying a strong C_3 signal in their enamel likely fed mainly on woody plants (trees, shrubs,
683 bushes) in woodlands, and possibly on C_3 sedges in humid habitats. They are usually
684 classified as browsers. Complicating factors of paleodietary reconstructions include the
685 potential consumption of CAM plants (mostly succulents in arid habitats and epiphytic plants
686 in closed forests) and C_4 dicot woody vegetation (e.g., shrubs of the family
687 Amaranthaceae/Chenopodiaceae). However, the classification of mammals using the
688 dichotomy between C_3 browsers and C_4 grazers inferred from $\delta^{13}\text{C}$ values is generally
689 confirmed by ecomorphological and dental wear studies¹⁰¹. $\delta^{13}\text{C}$ data of *P. robustus* are
690 intermediate between the C_4 pole and the C_3 pole, but closer to the latter, indicating a
691 preference of this hominin for the C_3 wooded and/or humid component of its habitat.

692 The enamel $\delta^{13}\text{C}$ data of the herbivorous mammals found at the Malapa site with *A. sediba*
693 indicate an environment dominated by C_4 plants, presumably grasses, and a few species
694 consuming C_3 plants, presumably woody plants²⁵. The pattern is therefore similar to the one
695 observed in the *P. robustus*-bearing sites, indicating a preference of *A. sediba* for the C_3
696 component, presumably woodland, of the otherwise C_4 grass-dominated landscapes.

697 **Ecomorphology and community structures:** Reed¹⁰³ conducted an analysis of the
698 ecological diversity of modern and past faunal communities by quantifying trophic and
699 locomotor adaptive traits of mammals. She found evidence that *P. robustus* inhabited mosaic
700 environments including both woodlands and grasslands, always close to a water source. She
701 also detected a pattern of more open habitats throughout the Swartkrans sequence. This
702 observation supports the information provided by $\delta^{13}\text{C}$ values of the herbivorous mammals
703 that, based on our data compilation, generally indicate more C_4 plants in the landscapes,
704 presumably grasses adapted to open and dry environments (Fig. 3B). de Ruiter et al.¹⁰⁴
705 conducted a correspondence analysis using the relative abundances of the different groups of
706 mammals classified as woodland-adapted and grassland-adapted based on stable carbon
707 isotopes and uniformitarian comparisons to extant relatives. They observed that the relative
708 abundance of *P. robustus* follows relative abundances of woodland-adapted species and is
709 negatively correlated to the relative abundances of grassland-adapted species. Bishop et al.¹⁰⁵
710 conducted an ecomorphological analysis of bovid postcrania from Sterkfontein Member 5B
711 "Oldowan Infill". They concluded that most bovid species were adapted to open grasslands,

712 and they reconstructed the environment as dominated by grasslands but with a nearby more
713 wooded component. Kuman & Clarke¹⁰⁶ suggested that the absence of *P. robustus* in
714 Sterkfontein Member 5 West could be linked to a drier local habitat without water-dependent
715 species. Overall, those studies indicate that grasslands were important and likely predominant
716 in the environments occupied by *P. robustus*, but always with a more wooded and humid
717 component nearby. The ecological data gained from multiple lines of evidence suggest that *P.*
718 *robustus* preferred that woodland and/or humid component.

719 **Combining the multiple lines of evidence:** based on the aforementioned evidence, we
720 interpret *P. robustus* as a species that was overall ecologically variable (eurytopic), especially
721 in terms of dietary resources, but with a long-lasting preference for the C₃ wooded or humid
722 components of the environments otherwise dominated by C₄ dry-adapted plants. Such a
723 selective feeding behavior, with scarce components of the vegetation that are over-represented
724 in the diet of an animal is frequently observed in extant mammals. For example, extant
725 geladas (*Theropithecus gelada*) from the Guassa Plateau in the Highlands of Ethiopia rely
726 extensively on forbs (ca. 38 % of annual diet, and up to 61 % of monthly diet) although those
727 preferred forbs represent only 8 % of ground cover¹⁰⁷. A variable C₃-dominated diet,
728 including both hard and tough food items, and displaying strong seasonal or inter-annual
729 variations, is supported by the stable carbon and oxygen isotopes, the dental microwear
730 textures, and the overall morphological adaptive traits displayed by *P. robustus*. The robust
731 craniomandibular and dental traits appear as a reasonable compromise to process efficiently
732 an extremely diversified diet including numerous tough parts of plants along with some hard
733 foods, and probably a lot of small food items that had to be eaten in small bites, with some
734 exogenous grit particulates adhering (e.g., termites, grass roots).

735 The preference of *P. robustus* for habitats dominated by C₃ plants, either in woodlands or in
736 humid environments, is well corroborated by the data gained from the study of other animals,
737 indicating large quantities of C₄ vegetation, but always with a more wooded component and
738 the nearby presence of a water source. Frequent exploitation of the C₄ food resources in the
739 more open component of the landscapes is demonstrated by the stable carbon isotopes that
740 indicate a significant, but not dominant, C₄ component in the diet. Possible use of bone tools
741 and prehensile hands would have enabled *P. robustus* to access a great variety of foods in
742 both wooded and open habitats. *Paranthropus robustus* could be best characterized as an
743 ecotonic species, exploiting intermediate habitats where the edge effect is maximized,
744 enabling it to forage on a maximal variety of foods in both wooded and open habitats within a
745 limited area, while keeping access to secure shelters in woodlands. Such an ecology is
746 displayed by the forest hog (*Hylochoerus meinertzhageni*) that strongly depends on wooded
747 humid forests for shelter, food, and water, but also frequently exploits open grasslands for
748 additional plant resources¹⁰⁸. Data are scarcer for *A. sediba* but the multiple aforementioned
749 lines of evidence suggest an even stronger preference for C₃ wooded habitats compared to *P.*
750 *robustus*. It is worth noting that similar preference for the C₃ component, presumably
751 woodlands, in overall C₄ grass-dominated landscapes is also documented in several other
752 hominin species from eastern Africa (e.g.,^{109,110}).

753 **Extinction of *Paranthropus robustus***

754 It appears likely that the last documented occurrence of *P. robustus* is dated ca. 0.9 Ma, or
755 even later (see Extended Data Table 1). Indeed, multiple lines of dating evidence point to a

756 young age of Swartkrans Member 3, likely around 0.9 Ma, but possibly as young as 0.6 Ma. It
757 is also worth keeping in mind the frequency of artificial range truncation of extinct taxa, often
758 called the Signor and Lipps effect¹¹¹: due to the imperfect nature of the fossil record, the
759 extinction date of a particular taxon is most probably more recent than the last fossil
760 occurrence of this taxon. Bearing in mind that those authors formulated this caution based on
761 the near-continuous and precisely-dated marine paleontological record, the Signor and Lipps
762 effect is even more pertinent when considering extinction dates based on the spatio-
763 temporally biased continental fossil record of terrestrial faunas (see details in White¹¹²). This
764 dating uncertainty most probably applies to *P. robustus* as its known geographic distribution
765 is extremely small. Most of the *P. robustus*-bearing sites are located within a circle of ca. 3
766 km radius, and only Gondolin is located a bit further north, around 25 km from Swartkrans
767 and Sterkfontein. A circle of 12.5 km radius, encompassing all the known occurrences of *P.*
768 *robustus*, would therefore represent a distribution area of ca. 500 km². Large mammals tend to
769 have much larger geographic distributions. For comparison, even the extant species of African
770 great apes with the smallest geographic distribution, the critically endangered eastern gorilla
771 (*Gorilla beringei*), is found over an area of ca. 70000 km². Other great apes have much larger
772 distributions (*G. gorilla*: over 700000 km²; *Pan paniscus*: ca. 156000 km²; *Pan troglodytes*:
773 over 2600000 km²; all data from the IUCN website, <http://www.iucnredlist.org/>). It is
774 therefore most likely that the real distribution area of *P. robustus* was much larger than what
775 is currently sampled by the available fossil record, making the true last occurrence of the
776 species unlikely to be sampled, and the real extinction date of the species likely younger than
777 0.9 Ma.

778 The fossil record of South Africa indicates that numerous species became extinct during the
779 Pleistocene. However, the paucity of the record after 1.4 Ma seriously hinders our
780 understanding of the pattern and timing of the extinctions. Middle Pleistocene faunas such as
781 those of Florisbad (ca. 0.25 Ma) are almost entirely composed of species that are similar to
782 the extant species whereas older faunas (e.g., Cornelia at ca. 1 Ma or Elandsfontein at 1 Ma-
783 0.6 Ma) contain a significant proportion of extinct species (e.g., ¹¹³). Neither a precise date
784 nor a time interval (1 Ma-0.5 Ma vs. later during the Pleistocene) can be constrained for the
785 extinction of those species based on their currently available fossil records.

786 Our new marine record, as well as previously published terrestrial records, are indicative of a
787 clear trend through time toward more open and drier landscapes in the Limpopo catchment.
788 Given that *P. robustus* preferentially thrived in non-dominant C₃ component of its
789 environment (either woodland or humid grassland), and that its diet was dominated by C₃
790 plants-derived food items, including occasional hard objects, we assume that the regional
791 trend toward a more arid hydroclimate after 1 Ma and the marked precessional variability
792 impacted the abundance of this species and its resilience to environmental changes. As
793 regional hydroclimate became drier, the wooded and humid environments favored by *P.*
794 *robustus* likely became progressively scarcer, strongly impacting the fitness and survival of
795 the populations of mammals depending on such habitats for food, water, and shelter. We
796 propose a speculative but plausible scenario inspired from the theoretical work by Foley²⁷.
797 According to this scenario, the geographic ranges of taxa adapted to woodlands and humid
798 habitats, including *P. robustus*, contracted and expanded according to the precessional ~21
799 kyr dry and wet cycles. During the multi-millennial dry periods, the range of populations of
800 those taxa contracted and often became fragmented. The resulting isolated populations were
801 especially prone to local extinction through increased competition and predation induced by

802 the lack of sufficient and suitable food, water, and shelter resources. During multi-millennial
803 wet periods, preferred woodland and humid habitats would have expanded again and the
804 surviving populations would have thrived again and expanded into their previously occupied
805 range, replacing locally extinct populations. The long term trend to aridity, as inferred from
806 our marine record, implies that dry periods became more and more drastic through time,
807 increasing the likelihood for local extinction of numerous local populations, until the
808 extinction of the last remaining local population, and therefore the extinction of the species.
809 Thus both long-term state and the extreme precessional changes in hydroclimate could have
810 impacted the evolution of *P. robustus*. A recent synthesis on factors involved in the extinction
811 in large mammals, spanning three continents and the whole Cenozoic period, concluded that
812 abiotic changes, such as climatic changes, were key players in the extinctions of species²⁶.

813 **What of *Homo*?** Several authors (reviewed in Wood & Strait¹¹⁴) suggested that strong
814 morphological, behavioral, and ecological differences between *P. robustus* and the
815 contemporary *Homo* gave an evolutionary advantage to the latter over the former. Some
816 authors therefore related those differences to the extinction of *P. robustus* while *Homo* did not
817 go extinct and remained extremely widespread in Africa and beyond. Strikingly different
818 relative abundances of those two taxa do suggest they were occupying separate ecological
819 niches in the sites where they co-occur (Swartkrans 96 % *P. robustus*, 4 % *Homo*; Drimolen
820 84 % *P. robustus* 16 % *Homo*, according to Moggi-Cecchi et al.¹¹⁵). However, those scenarios
821 are speculative and clearly out of the scope of our paper that is focused on *P. robustus*.
822 Regardless of any potential evolutionary advantage of *Homo* over *P. robustus*, whether or not
823 *Homo* went extinct locally in the Limpopo catchment during the aridification period is
824 meaningless to its subsequent evolutionary history. Remains of *Homo* are indeed known in
825 other parts of South Africa around 1 Ma (e.g., Elandsfontein¹¹⁶; Cornelia-Uitzoek¹¹⁷), as well
826 as in other parts of Africa^{118,119}, which would have made any local extinction counterbalanced
827 by subsequent dispersals from other regions. The survival of *Homo* could plausibly be
828 explained solely through plain contingency, especially as recent literature indicates a
829 eurytopic ecology for both *Homo* and *Paranthropus* (Wood & Strait¹¹⁴; our synthesis).

830

831

832

833

834

835 **Online Content** Methods, along with any additional Extended Data display items and

836 Source Data, are available in the online version of the paper; references unique to

837 these sections appear only in the online paper.

838

839

840

841

842
843
844
845
846
847
848
849

850 Methods references:

- 851 32. Page, E.S. Continuous Inspection Schemes. *Biometrika* **41**, 100–115 (1954).
852 33. García-Comas, C. *et al.* Zooplankton long-term changes in the NW Mediterranean
853 Sea: Decadal periodicity forced by winter hydrographic conditions related to large-
854 scale atmospheric changes? *J. Marine Syst.* **87**, 216–226 (2011).
855 34. Ibanez, F., Fromentin, J.M. & Castel, J. Application of the cumulated function to the
856 processing of chronological data in oceanography. *C. R. Acad. Sci. III-Vie* **316**, 745–
857 748 (1993).
858 35. Maher, L. J., Jr. Nomograms for computing 0.95 confidence limits of pollen data. *Rev.*
859 *Palaeobot. Palyn.* **13**, 85–93 (1972).
860 36. Lisiecki, L. E. & Raymo, M. E. A Pliocene-Pleistocene stack of 57 globally
861 distributed benthic $\delta^{18}\text{O}$ records. *Paleoceanography* **20**, PA1003 (2005).
862 37. Paillard, D., Labeyrie, L. D. & Yiou, P. AnalySeries 1.0: Macintosh program performs
863 time-series analysis. *EOS Trans. Am. Geophys. Un.* **77**, 379 (1996).
864 38. Barker, S., Greaves, M. & Elderfield, H. A study of cleaning procedures used for
865 foraminiferal Mg/Ca paleothermometry. *Geochem. Geophys. Geosyst.* **4**, 8407 (2003).
866 39. de Villiers, S., Greaves, M. & Elderfield, H. An intensity ratio calibration method for
867 the accurate determination of Mg/Ca and Sr/Ca of marine carbonates by ICP-AES.
868 *Geochem. Geophys. Geosyst.* **3**, 2001GC000169 (2002).
869 40. Anand, P., Elderfield, H. & Conte, M. H. Calibration of Mg/Ca thermometry in
870 planktonic foraminifera from a sediment trap time series. *Paleoceanography* **18**, 1050
871 (2003).
872 41. Hemleben, C., Spindler, M. & Erson, O. R. *Modern Planktonic Foraminifera*
873 (Springer-Verlag, 1989).
874 42. Kennett, J. P. & Srinivasan, M. S. *Neogene Planktonic Foraminifera: a Phylogenetic*
875 *Atlas* (Hutchinson Ross, 1983).
876 43. Guiot, J. & de Vernal, A. in *Proxies in Late Cenozoic Paleoceanography* (eds Hillaire-
877 Marcel, C. & de Vernal, A.) 523–563 (Elsevier, 2007).
878 44. Kucera, M. in *Proxies in Late Cenozoic Paleoceanography* (eds Hillaire-Marcel, C. &
879 de Vernal, A.) 213–262 (Elsevier, 2007).
880 45. Barrows, T. T. & Juggins, S. Sea-surface temperatures around the Australian margin
881 and Indian Ocean during the Last Glacial Maximum. *Quat. Sci. Rev.* **24**, 1017–1047
882 (2005).
883 46. Kucera, M. *et al.* Reconstruction of sea-surface temperatures from assemblages of
884 planktonic foraminifera: multi-technique approach based on geographically
885 constrained calibration data sets and its application to glacial Atlantic and Pacific
886 Oceans. *Quat. Sci. Rev.* **24**, 951–998 (2005).
887 47. Von Storch, H. & Zwiers, F. W. *Statistical Analysis in Climate Research* (Cambridge
888 University Press, 1999).
889 48. Roche, D. M. $\delta^{18}\text{O}$ water isotope in the iLOVECLIM model (version 1.0)–Part 1:
890 Implementation and verification. *Geosci. Model Dev.* **6**, 1481–1491 (2013).
891 49. Roche, D. M. & Caley, T. $\delta^{18}\text{O}$ water isotope in the iLOVECLIM model (version
892 1.0)–Part 2: Evaluation of model results against observed $\delta^{18}\text{O}$ in water samples.
893 *Geosci. Model Dev.* **6**, 1493–1504 (2013).
894 50. Caley, T. & Roche, D. M. $\delta^{18}\text{O}$ water isotope in the iLOVECLIM model (version
895 1.0)–Part 3: A palaeo-perspective based on present-day data–model comparison for
896 oxygen stable isotopes in carbonates. *Geosci. Model Dev.* **6**, 1505–1516 (2013).

- 897 51. Caley, T., Roche, D. M., & Renssen, H. Orbital Asian summer monsoon dynamics
898 revealed using an isotope-enabled global climate model. *Nat. Commun.* **5**, 5371
899 (2014).
- 900 52. Collins, J. A. *et al.* Rapid termination of the African Humid Period triggered by
901 northern high-latitude cooling. *Nat. Commun.* **8**, 1372 (2017).
- 902 53. Grine, F. E. & Daegling, D. J. Functional morphology, biomechanics and the
903 retrodiction of early hominin diets. *C. R. Palevol* **16**, 613–631 (2017).
- 904 54. Wood, B. & Schroer, K. in *Human Paleontology and Prehistory. Contributions in*
905 *Honor of Yoel Rak* (eds Marom, A. & Hovers, E.) 95–107 (Springer, 2017).
- 906 55. Patterson, D. B., Faith, J. T., Bobe, R. & Wood, B. Regional diversity patterns in
907 African bovids, hyaenids, and felids during the past 3 million years: the role of
908 taphonomic bias and implications for the evolution of *Paranthropus*. *Quat. Sci. Rev.*
909 **96**, 9–22 (2014).
- 910 56. Grine, F. E. (ed) *Evolutionary History of the “Robust” Australopithecines* (Aldine de
911 Gruyter, 1988).
- 912 57. Strait D. S. *et al.* Viewpoints: Diet and dietary adaptations in early hominins: the hard
913 food perspective. *Am. J. Phys. Anthropol.* **151**, 339–355 (2013).
- 914 58. Smith, A. L. *et al.* The feeding biomechanics and dietary ecology of *Paranthropus*
915 *boisei*. *Anat. Rec.* **298**, 145–167 (2015).
- 916 59. Rabenold, D. & Pearson, O. M. Abrasive, silica phytoliths and the evolution of thick
917 molar enamel in primates, with implications for the diet of *Paranthropus boisei*. *PLOS*
918 *ONE* **6**, e28379 (2011).
- 919 60. Scott, J. E., McAbee, K. R., Eastman, M. M. & Ravosa, M. J. Experimental
920 perspective on fallback foods and dietary adaptations in early hominins. *Biol. Letters*
921 **10**, 20130789 (2014).
- 922 61. Ungar, P. S., Grine, F. E. & Teaford, M. F. Dental microwear and diet of the Plio-
923 Pleistocene hominin *Paranthropus boisei*. *PLOS ONE* **3**, e2044 (2008).
- 924 62. Cerling, T. E. *et al.* Diet of *Paranthropus boisei* in the early Pleistocene of East
925 Africa. *Proc. Natl Acad. Sci. USA* **108**, 9337–9341 (2011).
- 926 63. King, R. A. *Using Ailuropoda melanoleuca as a Model Species for Studying the*
927 *Ecomorphology of Paranthropus*. Master thesis, Marshall University (2014).
- 928 64. Weng, Z. Y. *et al.* Giant panda's tooth enamel: structure, mechanical behavior and
929 toughening mechanisms under indentation. *J. Mech. Behav. Biomed.* **64**, 125–138
930 (2016).
- 931 65. Ungar, P. S. & Hlusko, L. J. The evolutionary path of least resistance. *Science* **353**,
932 29–30 (2016).
- 933 66. Lucas, P. W. *Dental Functional Morphology: How Teeth Work* (Cambridge University
934 Press, 2004).
- 935 67. Souron, A. in *Ecology, Conservation and Management of Wild Pigs and Peccaries*
936 (eds Melletti, M. & Meijaard, E.) 29–38 (Cambridge University Press, 2017).
- 937 68. Ledogar, J. A. *et al.* Mechanical evidence that *Australopithecus sediba* was limited in
938 its ability to eat hard foods. *Nat. Commun.* **7**, 10596 (2016).
- 939 69. Daegling, D. J., Carlson, K. J., Tafforeau, P., de Ruiter, D. J., & Berger, L. R.
940 Comparative biomechanics of *Australopithecus sediba* mandibles. *J. Hum. Evol.* **100**,
941 73–86 (2016).
- 942 70. Grine, F. E. & Susman, R. L. Radius of *Paranthropus robustus* from member 1,
943 Swartkrans formation, *South Africa*. *Am. J. Phys. Anthropol.* **84**, 229–248 (1991).
- 944 71. Patel, B. A. The hominoid proximal radius: re-interpreting locomotor behaviors in
945 early hominins. *J. Hum. Evol.* **48**, 415–432 (2005).

- 946 72. Susman, R. L. Hand of *Paranthropus robustus* from Member 1, Swartkrans: fossil
947 evidence for tool behavior. *Science* **240**, 781–784 (1988).
- 948 73. Backwell, L. R. & d’Errico, F. Additional evidence on the early hominid bone tools
949 from Swartkrans with reference to spatial distribution of lithic and organic artefacts. *S.
950 Afr. J. Sci.* **99**, 259–267 (2003).
- 951 74. Backwell, L. R. & d’Errico, F. Early hominid bone tools from Drimolen, South Africa.
952 *J. Archaeol. Sci.* **35**, 2880–2894 (2008).
- 953 75. d’Errico, F. & Backwell, L. R. Assessing the function of early hominin bone tools. *J.
954 Archaeol. Sci.* **36**, 1764–1773 (2009).
- 955 76. Churchill, S. E. *et al.* The upper limb of *Australopithecus sediba*. *Science* **340**,
956 1233477 (2013).
- 957 77. Rein, T. R., Harrison, T., Carlson, K. J. & Harvati, K. Adaptation to suspensory
958 locomotion in *Australopithecus sediba*. *J. Hum. Evol.* **104**, 1–12 (2017).
- 959 78. Macho, G. *in Trends in Biological Anthropology*. Volume 1 (eds Gerdau-Radonić, K.
960 & McSweeney, K.) 1–10 (Oxbow Books, 2015).
- 961 79. Tseng, Z. J. Connecting Hunter-Schreger Band microstructure to enamel microwear
962 features: new insights from durophagous carnivores. *Acta Palaeontol. Pol.* **57**, 473–
963 484 (2012).
- 964 80. Alloing-Séguier, L., Lihoreau, F., Boisserie, J.-R., Charruault, A.-L., Orliac, M. &
965 Tabuce, R. Enamel microstructure evolution in anthracotheres (Mammalia,
966 Cetartiodactyla) and new insights on hippopotamoid phylogeny. *Zool. J. Linn. Soc.*
967 *171*, 668–695 (2014).
- 968 81. Constantino, P. J., Borrero-Lopez, O., Pajares, A. & Lawn, B. R. Simulation of enamel
969 wear for reconstruction of diet and feeding behavior in fossil animals: a
970 micromechanics approach. *BioEssays* **38**, 89–99 (2016).
- 971 82. Towle, I., Irish, J. D. & De Groote, I. Behavioral inferences from the high levels of
972 dental chipping in *Homo naledi*. *Am. J. Phys. Anthropol.* **164**, 184–192 (2017).
- 973 83. Sponheimer, M. *et al.* Isotopic evidence for dietary variability in the early hominin
974 *Paranthropus robustus*. *Science* **314**, 980–982 (2006).
- 975 84. Sponheimer, M. *et al.* Hominins, sedges, and termites: new carbon isotope data from
976 the Sterkfontein valley and Kruger National Park. *J. Hum. Evol.* **48**, 301–312 (2005).
- 977 85. Sponheimer, M. & Lee-Thorp, J. A. Differential resource utilization by extant great
978 apes and australopithecines: towards solving the C₄ conundrum. *Comp. Biochem.
979 Phys. A* **136**, 27–34 (2003).
- 980 86. Sponheimer, M. *in The Paleobiology of Australopithecus* (eds Reed, K. E., Fleagle, J.
981 G. & Leakey, R. E.) 225–233 (Springer, 2013).
- 982 87. Dominy, N. J., Vogel, E. R., Yeakel, J. D., Constantino, P. & Lucas, P. W. Mechanical
983 properties of plant underground storage organs and implications for dietary models of
984 early hominins. *Evol. Biol.* **35**, 159–175 (2008).
- 985 88. Yeakel, J. D., Dominy, N. J., Koch, P. L. & Mangel, M. Functional morphology,
986 stable isotopes, and human evolution: a model of consilience. *Evolution* **68**, 190–203
987 (2014).
- 988 89. Sponheimer, M. & Lee-Thorp, J. A. Oxygen isotopes in enamel carbonate and their
989 ecological significance. *J. Archaeol. Sci.* **26**, 723–728 (1999).
- 990 90. Levin, N. E., Cerling, T. E., Passey, B. H., Harris, J. M. & Ehleringer, J. R. A stable
991 isotope aridity index for terrestrial environments. *Proc. Natl Acad. Sci. USA* **103**,
992 11201–11205 (2006).
- 993 91. Faith, J. T. Paleodietary change and its implications for aridity indices derived from
994 $\delta^{18}\text{O}$ of herbivore tooth enamel. *Palaeogeogr. Palaeoclimatol. Palaeoecol.* **490**, 571–
995 578 (2018).

- 996 92. Lee-Thorp, J. A., Sponheimer, M., Passey, B. H., de Ruiter, D. J. & Cerling, T. E.
997 Stable isotopes in fossil hominin tooth enamel suggest a fundamental dietary shift in
998 the Pliocene. *Philos. T. Roy. Soc. B* **365**, 3389–3396 (2010).
999 93. Souron, A., Balasse, M. & Boisserie, J.-R. Intra-tooth isotopic profiles of canines from
1000 extant *Hippopotamus amphibius* and late Pliocene hippopotamids (Shungura
1001 Formation, Ethiopia): insights into the seasonality of diet and climate. *Palaeogeogr.*
1002 *Palaeoclimatol. Palaeoecol.* **342–343**, 97–110 (2012).
1003 94. Sponheimer, M., de Ruiter, D., Lee-Thorp, J. & Späth, A. Sr/Ca and early hominin
1004 diets revisited: new data from modern and fossil tooth enamel. *J. Hum. Evol.* **48**, 147–
1005 156 (2005).
1006 95. Ungar, P. S. & Sponheimer, M. The diets of early hominins. *Science* **334**, 190–193
1007 (2011).
1008 96. Grine, F. E., Sponheimer, M., Ungar, P. S., Lee-Thorp, J. & Teaford, M. F. Dental
1009 microwear and stable isotopes inform the paleoecology of extinct hominins. *Am. J.*
1010 *Phys. Anthropol.* **148**, 285–317 (2012).
1011 97. Ungar, P. S., Scott, J. R. & Steininger, C. M. Dental microwear differences between
1012 eastern and southern African fossil bovids and hominins. *S. Afr. J. Sci.* **112**, 1–5
1013 (2016).
1014 98. Peterson, A. S. *Dental Microwear Textures of Paranthropus robustus from*
1015 *Kromdraai, Drimolen, and an Enlarged Sample from Swartkrans: Ecological and*
1016 *Intraspecific Variation*. Master thesis, University for Arkansas (2017).
1017 99. Lee-Thorp, J. A., van der Merwe, N. J. & Brain, C. K. Diet of *Australopithecus*
1018 *robustus* at Swartkrans from stable carbon isotopic analysis. *J. Hum. Evol.* **27**, 361–
1019 372 (1994).
1020 100. Lee-Thorp, J., Thackeray, J. F. & van der Merwe, N. The hunters and the
1021 hunted revisited. *J. Hum. Evol.* **39**, 565–576 (2000).
1022 101. Steininger, C. M. *The dietary behaviour of early Pleistocene bovids from*
1023 *Cooper's Cave and Swartkrans, South Africa*. PhD thesis, University of the
1024 Witwatersrand (2011).
1025 102. Adams, J. W. Stable carbon isotope analysis of fauna from the Gondolin GD 2
1026 fossil assemblage, South Africa. *Ann. Ditsong Natl Mus. Nat. Hist.* **2**, 1–5 (2012).
1027 103. Reed, K. E. Early hominid evolution and ecological change through the
1028 African Plio-Pleistocene. *J. Hum. Evol.* **32**, 289–322 (1997).
1029 104. de Ruiter, D. J., Sponheimer, M. & Lee-Thorp, J. A. Indications of habitat
1030 association of *Australopithecus robustus* in the Bloubaank Valley, South Africa. *J.*
1031 *Hum. Evol.* **55**, 1015–1030 (2008).
1032 105. Bishop, L. C., Pickering, T., Plummer, T. & Thackeray, F. Paleoenvironmental
1033 setting for the Oldowan industry at Sterkfontein. *Paper presented at the XVth*
1034 *International Congress of the International Union for Quaternary Research, The*
1035 *Environmental Background to Hominid Evolution in Africa, Durban* (1999).
1036 106. Kuman, K. & Clarke, R. J. Stratigraphy, artefact industries and hominid
1037 associations for Sterkfontein, Member 5. *J. Hum. Evol.* **38**, 827–847 (2000).
1038 107. Fashing, P. J., Nguyen, N., Venkataraman, V. V. & Kerby, J. T. Gelada feeding
1039 ecology in an intact ecosystem at Guassa, Ethiopia: variability over time and
1040 implications for theropit and hominin dietary evolution. *Am. J. Phys. Anthropol.*
1041 **155**, 1–16 (2014).
1042 108. d'Huart, J.-P. in *Pigs, Peccaries, and Hippos : Status Survey and Conservation*
1043 *Action Plan* (ed. Oliver, W. L. R.) 84–92 (IUCN, 1993).

- 1044 109. Quinn, R. L. *et al.* Pedogenic carbonate stable isotopic evidence for wooded
1045 habitat preference of early Pleistocene tool makers in the Turkana Basin. *J. Hum.*
1046 *Evol.* **65**, 65–78 (2013).
- 1047 110. Robinson, J. R., Rowan, J., Campisano, C. J., Wynn, J. G. & Reed, K. E.. Late
1048 Pliocene environmental change during the transition from *Australopithecus* to *Homo*.
1049 *Nature Ecol. Evol.* **1**, 0159 (2017).
- 1050 111. Signor, P. W., III & Lipps, J. H. in *Geological Implications of Impacts of*
1051 *Large Asteroids and Comets on the Earth* (eds Silver, L. T. & Schultz, P. H.) 291–296
1052 (The Geological Society of America, 1982).
- 1053 112. White, T. D. in *Paleoclimate and Evolution, with Emphasis on Human Origins*
1054 (eds Vrba, E. S., Denton, G. H., Partridge, T. C. & Burckle, L. H.) 369–384 (Yale
1055 University Press, 1995).
- 1056 113. Codron, D., Brink, J. S., Rossouw, L. & Clauss, M. The evolution of ecological
1057 specialization in southern African ungulates: competition-or physical environmental
1058 turnover? *Oikos* **117**, 344–353 (2008).
- 1059 114. Wood, B. & Strait, D. Patterns of resource use in early *Homo* and
1060 *Paranthropus*. *J. Hum. Evol.* **46**, 119–162 (2004).
- 1061 115. Moggi-Cecchi, J., Menter, C., Boccone, S. & Keyser, A. Early hominin dental
1062 remains from the Plio-Pleistocene site of Drimolen, South Africa. *J. Hum. Evol.* **58**,
1063 374–405 (2010).
- 1064 116. Klein, R. G., Avery, G., Cruz-Uribe, K. & Steele, T. E. The mammalian fauna
1065 associated with an archaic hominin skullcap and later Acheulean artifacts at
1066 Elandsfontein, Western Cape Province, South Africa. *J. Hum. Evol.* **52**, 164–186
1067 (2007).
- 1068 117. Brink, J. S. *et al.* First hominine remains from a~ 1.0 million year old bone bed
1069 at Cornelia-Uitzoek, Free State Province, South Africa. *J. Hum. Evol.* **63**, 527–535
1070 (2012).
- 1071 118. Asfaw, B. *et al.* Remains of *Homo erectus* from Bouri, Middle Awash,
1072 Ethiopia. *Nature* **416**, 317–320 (2002).
- 1073 119. Abbate, E. *et al.* A one-million-year-old *Homo* cranium from the Danakil
1074 (Afar) Depression of Eritrea. *Nature* **393**, 458–460 (1998).
- 1075 120. Bahr, A. *et al.* Deciphering bottom current velocity and paleoclimate signals
1076 from contourite deposits in the Gulf of Cádiz during the last 140 kyr: an inorganic
1077 geochemical approach. *Geochem. Geophys. Geosyst.* **15**, 3145–3160 (2014).
- 1078 121. Adegbeie, A. T., Schneider, R. R., Röhl, U. & Wefer, G. Glacial millennial-
1079 scale fluctuations in central African precipitation recorded in terrigenous sediment
1080 supply and freshwater signals offshore Cameroon. *Palaeogeogr. Palaeoclimatol.*
1081 *Palaeoecol.* **197**, 323–333 (2003).
- 1082 122. Dickson, A. J., Leng, M. J., Maslin, M. A. & Röhl, U. Oceanic, atmospheric
1083 and ice-sheet forcing of South East Atlantic Ocean productivity and South African
1084 monsoon intensity during MIS-12 to 10. *Quat. Sci. Rev.* **29**, 3936–3947 (2010).
- 1085 123. Revel, M. *et al.* 20,000 years of Nile River dynamics and environmental
1086 changes in the Nile catchment area as inferred from Nile upper continental slope
1087 sediments. *Quat. Sci. Rev.* **130**, 200–221 (2015).
- 1088 124. Ziegler, M. *et al.* Development of Middle Stone Age innovation linked to rapid
1089 climate change. *Nat. Commun.* **4**, 1905 (2013).
- 1090 125. Rohling, E. J. *et al.* Sea-level and deep-sea-temperature variability over the
1091 past 5.3 million years. *Nature* **508**, 477–482 (2014).

- 1092 126. IAEA. *Isotope Hydrology Information System, The ISOHIS Database*
1093 (available at: <http://www.iaea.org/water>, 2006, last access: 8 March 2012).
- 1094 127. Risi, C., Bony, S. & Vimeux, F. Influence of convective processes on the
1095 isotopic composition ($\delta^{18}\text{O}$ and δD) of precipitation and water vapor in the tropics: 2.
1096 Physical interpretation of the amount effect. *J. Geophys. Res.* **113**, D19306 (2008).
- 1097 128. Stock, W. D., Chuba, D. K. & Verboom, G. A. Distribution of South African
1098 C_3 and C_4 species of Cyperaceae in relation to climate and phylogeny. *Austral Ecol.*
1099 **29**, 313–319 (2004).
- 1100 129. Dupont, L. M. & Kuhlmann, H. Glacial-interglacial vegetation change in the
1101 Zambezi catchment. *Quat. Sci. Rev.* **155**, 127–135 (2017).
- 1102 130. Schrag, D. P. *et al.* The oxygen isotopic composition of seawater during the
1103 Last Glacial Maximum. *Quat. Sci. Rev.* **21**, 331–342 (2002).
- 1104 131. Sachse, D. *et al.* Molecular paleohydrology: interpreting the hydrogen-isotopic
1105 composition of lipid biomarkers from photosynthesizing organisms. *Annu. Rev. Earth*
1106 *Planet. Sci.* **40**, 221–249 (2012).
- 1107 132. Collins, J. A. *et al.* Estimating the hydrogen isotopic composition of past
1108 precipitation using leaf-waxes from western Africa. *Quat. Sci. Rev.* **65**, 88–101 (2013).
- 1109 133. Schefuß, E., Schouten, S., Jansen, J. F. & Sinninghe Damsté, J. S. African
1110 vegetation controlled by tropical sea surface temperatures in the mid-Pleistocene
1111 period. *Nature* **422**, 418–421 (2003).
- 1112 134. Grinsted, A. Moore, J. C. & Jevrejeva, S. Application of the cross wavelet
1113 transform and wavelet coherence to geophysical time series. *Nonlinear Process.*
1114 *Geophys.* **11**, 561–566 (2004).
- 1115 135. Schulz, M. & Mudelsee, M. REDFIT: estimating red-noise spectra directly
1116 from unevenly spaced paleoclimatic time series. *Comput. Geosci.* **28**, 421–426 (2002).
- 1117 136. Imbrie, J. *et al.* in *Milankovitch and Climate: Understanding the Response to*
1118 *Astronomical Forcing* (eds Berger, A. *et al.*) 269–305 (D. Reidel Publishing
1119 Company, 1984).
- 1120 137. Dirks, P. H. *et al.* Geological setting and age of *Australopithecus sediba* from
1121 southern Africa. *Science* **328**, 205–208 (2010).
- 1122 138. Pickering, R. *et al.* *Australopithecus sediba* at 1.977 Ma and implications for
1123 the origins of the genus *Homo*. *Science* **333**, 1421–1423 (2011).
- 1124 139. Berger, L. R., de Ruiter, D. J., Steininger, C. M. & Hancox, J. Preliminary
1125 results of excavations at the newly investigated Coopers D deposit, Gauteng, South
1126 Africa. *S. Afr. J. Sci.* **99**, 276–278 (2003).
- 1127 140. de Ruiter, D. J. *et al.* New *Australopithecus robustus* fossils and associated U-
1128 Pb dates from Cooper's cave (Gauteng, South Africa). *J. Hum. Evol.* **56**, 497–513
1129 (2009).
- 1130 141. Keyser, A. W., Menter, C. G., Moggi-Cecchi, J., Pickering, T. R. & Berger, L.
1131 R. Drimolen: a new hominid-bearing site in Gauteng, South Africa. *S. Afr. J. Sci.* **96**,
1132 193–197 (2000).
- 1133 142. Adams, J. W., Rovinsky, D. S., Herries, A. I. & Menter, C. G.
1134 Macromammalian faunas, biochronology and palaeoecology of the early Pleistocene
1135 Main Quarry hominin-bearing deposits of the Drimolen Palaeocave System, South
1136 Africa. *PeerJ* **4**, e1941 (2016).
- 1137 143. Thackeray, J. F., Kirschvink, J. L. & Raub, T. D. Palaeomagnetic analyses of
1138 calcified deposits from the Plio-Pleistocene hominid site of Kromdraai, South Africa:
1139 news & views. *S. Afr. J. Sci.* **98**, 537–540 (2002).

- 1140 144. Herries, A. I., Curnoe, D. & Adams, J. W. A multi-disciplinary seriation of
 1141 early *Homo* and *Paranthropus* bearing palaeocaves in southern Africa. *Quat. Int.* **202**,
 1142 14–28 (2009).
- 1143 145. Herries, A. I. & Adams, J. W. Clarifying the context, dating and age range of
 1144 the Gondolin hominins and *Paranthropus* in South Africa. *J. Hum. Evol.* **65**, 676–681
 1145 (2013).
- 1146 146. Braga, J., Fourvel, J.-B., Lans, B., Bruxelles, L. & Thackeray, J. F. in
 1147 *Kromdraai. A birthplace of Paranthropus in the Cradle of Humankind* (eds Braga, J. &
 1148 Thackeray, J. F.) 1–16 (SUN PRESS, 2016).
- 1149 147. Herries, A. I., Adams, J. W., Kuykendall, K. L. & Shaw, J. Speleology and
 1150 magnetobiostratigraphic chronology of the GD 2 locality of the Gondolin hominin-
 1151 bearing paleocave deposits, North West Province, South Africa. *J. Hum. Evol.* **51**,
 1152 617–631 (2006).
- 1153 148. Adams, J. W., Herries, A. I., Kuykendall, K. L. & Conroy, G. C. Taphonomy
 1154 of a South African cave: geological and hydrological influences on the GD 1 fossil
 1155 assemblage at Gondolin, a Plio-Pleistocene paleocave system in the Northwest
 1156 Province, South Africa. *Quat. Sci. Rev.* **26**, 2526–2543 (2007).
- 1157 149. Curnoe, D. K. A. *Contribution to the question of early Homo in southern*
 1158 *Africa: researches into dating, taxonomy and phylogeny reconstruction*. PhD thesis,
 1159 Australian National University (1999).
- 1160 150. Herries, A. I. & Shaw, J. Palaeomagnetic analysis of the Sterkfontein
 1161 palaeocave deposits: Implications for the age of the hominin fossils and stone tool
 1162 industries. *J. Hum. Evol.* **60**, 523–539 (2011).
- 1163 151. Granger, D. E. *et al.* New cosmogenic burial ages for Sterkfontein Member 2
 1164 *Australopithecus* and Member 5 Oldowan. *Nature* **522**, 85–88 (2015).
- 1165 152. Gibbon, R. J. *et al.* Cosmogenic nuclide burial dating of hominin-bearing
 1166 Pleistocene cave deposits at Swartkrans, South Africa. *Quat. Geochronol.* **24**, 10–15
 1167 (2014).
- 1168 153. Curnoe, D., Grün, R., Taylor, L. & Thackeray, F. Direct ESR dating of a
 1169 Pliocene hominin from Swartkrans. *J. Hum. Evol.* **40**, 379–391 (2001).
- 1170 154. Pickering, R., Kramers, J. D., Hancox, P. J., de Ruiter, D. J. & Woodhead, J. D.
 1171 Contemporary flowstone development links early hominin bearing cave deposits in
 1172 South Africa. *Earth Planet. Sc. Lett.* **306**, 23–32 (2011).
- 1173 155. Balter, V. *et al.* U-Pb dating of fossil enamel from the Swartkrans Pleistocene
 1174 hominid site, South Africa. *Earth Planet. Sc. Lett.* **267**, 236–246 (2008).
- 1175 156. Vrba, E. S. Some evidence of chronology and palaeoecology of Sterkfontein,
 1176 Swartkrans and Kromdraai from the fossil Bovidae. *Nature* **254**, 301–304 (1975).
- 1177 157. Vrba, E. S. in *L'environnement des hominidés au Plio-Pléistocène* (eds Beden,
 1178 M. *et al.*) 345–369 (Masson, 1985).
- 1179 158. Churcher, C. S. & Watson, V. Additional fossil Equidae from Swartkrans.
 1180 Swartkrans: a cave's chronicle of early man. *Pretoria: Transvaal Museum* **8**, 137–150
 1181 (1993).
- 1182 159. Blackwell, B. A. Problems associated with reworked teeth in electron spin
 1183 resonance (ESR) dating. *Quat. Sci. Rev.* **13**, 651–660 (1994).
- 1184 160. Steininger, C. Local ecological profile for *Paranthropus robustus* in South
 1185 Africa using stable carbon isotopes from associated bovid teeth. *Quat. Int.* **279**, 466
 1186 (2012).
- 1187
 1188
 1189

1190 **Extended data legends:**

1191

1192 **Extended Data Figure 1: $\ln(\text{Fe}/\text{Ca})$ as a proxy for Limpopo runoff.** Ca and Fe are both
1193 elements with complex and multiple origins in marine sediments. Fe could be related with
1194 redox variations, detrital and fluvial input, among others while Ca can be related with the
1195 biogenic fraction (foraminifera, nannofossils) and detrital input. In order to properly interpret
1196 the $\ln(\text{Fe}/\text{Ca})$ ratio at our study location we applied principal components analysis¹²⁰ (PCA).

1197 a) The first principal component (PC1) describes 66 % of the total variance for the entire site
1198 MD96-2048. The negative loadings for PC1 are Ca and Sr while all other elements (Al, Si, K,
1199 Ti, Fe and Zr) have positive loadings. Ca and Sr are elements associated with biogenic
1200 carbonate and are mainly related to presence of foraminifera. Element matrix correlation
1201 shows a strong positive linear correlation ($R > +0.70$) between Fe and typically detrital
1202 elements as Al, Si, Ti and K. Ca shows negative correlation with Fe ($R = -0.5$).

1203 b) $\ln(\text{Fe}/\text{Ca})$ show a strong correlation with PC1 ($R = 0.94$) and a strong relationship with
1204 Limpopo runoff proxies (Extended Data Fig. 3). Fe and Ti elements are related to terrigenous
1205 and siliciclastic components (heavy minerals, oxides) and the carbonate content (Ca) variation
1206 is mainly due to dilution by terrigenous sediment. $\ln(\text{Fe}/\text{Ca})$ is therefore a proxy of Limpopo
1207 runoff in agreement with previous studies in riverine basins along the African continent<sup>10,121-
1208 124</sup>.

1209 To confirm a weak influence of sea level changes on the Fe/Ca record we compared our \ln
1210 (Fe/Ca) record with the deep-water $\delta^{18}\text{O}$ component for relative sea level reconstructed by
1211 Rohling et al.,¹²⁵ (bottom on b)). Both records are plotted against the LR04 chronology.

1212 Visual inspection and statistical test do not support a dominant effect of sea level changes on
1213 the $\ln(\text{Fe}/\text{Ca})$ record ($R = 0.05$). PC3, that describes 11 % of the total variance for the entire
1214 site MD96-2048, is closely related to sea level changes. The negative loadings for PC3 are
1215 mainly Sr and to a lesser degree K and Ti while the main positive loadings are Zr and to a
1216 lesser degree Si.

1217

1218

1219 **Extended Data Figure 2: Control on the δD composition of precipitation in the Limpopo**

1220 **catchment.** a) Seasonal δD composition of precipitation and b) precipitation at Pretoria
1221 station¹²⁶ in comparison to the iLOVECLIM model results at the corresponding latitude and
1222 longitude^{48,49}. All data are centered around their annual average. Depleted δD values are
1223 indicative of increasing amounts of rainfall¹²⁷. c) Results of the transient simulation with the
1224 isotope enabled numerical climate model iLOVECLIM for the δD composition of
1225 precipitation and precipitation in the Limpopo catchment ($\sim -27.5^\circ\text{S}$ to -22°S and 30°E to
1226 36°E) over the last 150 kyr (Methods)⁵¹. Black curves show the results after filtering with a
1227 low pass filter. The δD composition of precipitation and precipitation amount in the Limpopo
1228 catchment are negatively correlated ($R = -0.63$, $p\text{-value} \ll 0.001$) over the last 150 kyr.
1229 Maxima of precipitation are phased with maxima in austral summer insolation at 30°S and
1230 lead to more depleted $\delta\text{D}_{\text{precipitation}}$ (amount effect).

1231

1232 **Extended Data Figure 3: Relationship between Limpopo runoff, local Southern**
1233 **Hemisphere insolation and the C_{31} n -alkane $\delta^{13}\text{C}$ record over the last 800 kyr.** a)

1234 Comparison between the $\ln(\text{Fe}/\text{Ca})$ XRF signal and austral summer local insolation at 30°S ³¹.
1235 b) Comparison between the $\ln(\text{Fe}/\text{Ca})$ XRF signal and the branched glycerol dialkyl glycerol
1236 tetraethers (brGDGT) concentration in the sediment¹⁵. brGDGT are commonly found in soil
1237 and can be attributed to Limpopo River runoff¹⁵. c) Comparison between the $\ln(\text{Fe}/\text{Ca})$ XRF
1238 signal and the C_{31} n -alkane $\delta^{13}\text{C}$ record¹⁶. More Limpopo River discharge is associated with
1239 more C_4 plant input and increase in austral summer insolation at 30°S . d) Comparison

1240 between inverted $\ln(\text{Fe}/\text{Ca})$ XRF signal and the accumulation rate (AR) of CaCO_3 as a
1241 measure of biogenic carbonate. The $\ln(\text{Fe}/\text{Ca})$ XRF record is not primarily controlled by
1242 dilution due to biological productivity ($R = 0.1$).
1243 A previous study on core MD96-2048 over the last 0.8 Ma interpreted shifts towards more
1244 depleted $\delta^{13}\text{C}_{\text{wax}}$ as potentially reflecting more humid conditions¹⁶. However, the anti-
1245 correlation between $\delta^{13}\text{C}_{\text{wax}}$ and $\delta\text{D}_{\text{wax}}$ values (Extended Data Fig. 4) in our study indicates
1246 that enriched $\delta^{13}\text{C}_{\text{wax}}$ values are associated with more humid conditions. Because C_4 plants in
1247 the Limpopo catchment are dominant in the interior (Fig. 1), we propose that more enriched
1248 $\delta^{13}\text{C}_{\text{wax}}$ values indicate a higher relative contribution from more upstream sources (more C_4)
1249 during times of high runoff compared to only downstream sources (more C_3) during low
1250 discharge. In addition, humid conditions would have favored the extension of sedge-rich
1251 vegetation (Cyperaceae, of which 20 to 60 % are C_4 plants in this region¹²⁸) in riverine
1252 swamps and floodplains along the river course, explaining the detected increase in
1253 Cyperaceae pollen at times of increased fluvial discharge (Fig. 2). Studies on sediments from
1254 the adjacent Zambezi catchment similarly suggest the extension of swampy sedge-rich
1255 vegetation including C_4 -Cyperaceae when river discharge was high and infer that more C_4
1256 plant waxes are exported to the ocean when flooding of floodplains occurs during rainfall
1257 maxima^{10,129}.

1258

1259 **Extended Data Figure 4: Relation between the $\delta^{13}\text{C}$ C_{31} n -alkanes record and the δD C_{31}**
1260 **n -alkanes record.** A. Correlation between the $\delta^{13}\text{C}$ C_{31} n -alkanes record and the δD C_{31} n -
1261 alkanes record with or without vegetation and ice volume correction (vc-ivf) over the last 2.14
1262 Ma ($n = 19$). An anti-correlation exists between the $\delta^{13}\text{C}$ and the δD signals of the C_{31} n -
1263 alkanes. The C_{31} n -alkane is used because it is the most abundant homologue in the samples.
1264 B. Raw $\delta^{13}\text{C}_{\text{wax}}$, $\delta\text{D}_{\text{wax}}$ data and $\delta\text{D}_{\text{wax}}$ adjusted for ice-volume and vegetation changes from
1265 core MD96-2048. Mean analytical uncertainties are indicated. a) $\delta^{13}\text{C}_{\text{wax}}$ of the C_{31}
1266 homologue (Castaneda et al.¹⁶ in light green and this study in dark green). b) $\delta\text{D}_{\text{wax}}$ of the C_{31}
1267 homologue. c) $\delta\text{D}_{\text{wax}}$ of the C_{31} homologue adjusted for ice volume changes (ivf) using a
1268 seawater $\delta^{18}\text{O}$ curve¹²⁵ and converting to δD assuming a Last Glacial Maximum (LGM)
1269 increase of 7.2‰. We use 7.2‰ because sediment pore water $\delta^{18}\text{O}$ and δD measurements
1270 suggest that the glacial ocean δD increase has a mean value of 7.2‰¹³⁰. We also adjusted the
1271 $\delta\text{D}_{\text{wax}}$ record for vegetation changes (vc) using published fractionation factors ($-123\text{‰} \pm 31\text{‰}$
1272 for C_3 trees, $-139\text{‰} \pm 27\text{‰}$ for C_4 grasses¹³¹) and the $\delta^{13}\text{C}_{\text{wax}}$ signal following the procedure
1273 developed by Collins et al.¹³². End-member $\delta^{13}\text{C}_{\text{wax}}$ values used for C_3 and C_4 vegetation were
1274 -36‰ and -21.5‰ , respectively¹³³. The error ranges for the vegetation fractionation factors
1275 are very large¹³¹. They derive from the compilation of a global dataset from individual plants
1276 which is not comparable to an ecosystem fractionation in a specific catchment such in the
1277 Limpopo that will fractionate with a much smaller uncertainty. As we, however, do not know
1278 the exact fractionation factor in the Limpopo catchment and regard the uncertainties from the
1279 global compilation as unrealistic for a specific ecosystem we refrained from propagating this
1280 uncertainty into the vegetation corrections. The vegetation and ice-volume adjusted $\delta\text{D}_{\text{wax}}$
1281 record is very similar to the unadjusted record, highlighting that the adjustments have a minor
1282 effect.

1283

1284 **Extended Data Figure 5: Statistical analyses for the $\ln \text{Fe}/\text{Ca}$ XRF record and PC1 SST**
1285 **record.** a) Spectral power for $\ln(\text{Fe}/\text{Ca})$ by wavelet analysis realized with the MatLab
1286 package of Grinsted et al.¹³⁴. The thick contour designates the 5 % significance level against
1287 red noise. Dash black lines indicate the variability at the precession, obliquity and eccentricity
1288 periods. b) Spectral analysis of $\ln \text{Fe}/\text{Ca}$ with REDFIT¹³⁵. Red line show the false-alarm level
1289 at the 95 % confidence interval. Spectral peaks exceeding the false-alarm level can be

1290 considered significant¹³⁵. c) Blackman-Tukey cross correlation between ln(Fe/Ca) XRF and
1291 ETP realized with the Analyseries software³⁷ over the last 2.14 Ma. ETP is constructed by
1292 normalizing and stacking Eccentricity, Tilt (obliquity) and negative Precession to evaluate
1293 coherence and phase (timing) relative to orbital extremes¹³⁶. Red curve shows the spectral
1294 power for ln Fe/Ca record. Black curve show the spectral power for ETP. The coherency
1295 (which varies between 0 and 1) is represented by the grey curve and gives the interval within
1296 which the spectrum is significant. In our case, the non-zero coherency is higher than 0.55 and
1297 is significant at the 95 % confidence interval (grey line). There are significant spectral peaks
1298 for eccentricity and precession but not for obliquity. The ln(Fe/Ca) XRF record and ETP are
1299 in phase at the 400 kyr period, the eccentricity leads by 16 kyr the ln(Fe/Ca) record at the 100
1300 kyr period and the ln(Fe/Ca) record is in anti-phase with negative precession (in-phase with
1301 positive precession) at the 19 and 23 kyr periods. The three statistical analyses are in
1302 agreement and indicate significant variability at the 400, 100, 23 and 19 kyr periods and
1303 insignificant variability at 41 kyr period. d) Comparison between the precessional component
1304 of the ln(Fe/Ca) record (Gaussian filter frequency 1/23 000; bandwidth: 5e-06) obtained with
1305 the Analyseries software³⁷ and the precession index. Maxima of the ln(Fe/Ca) precession
1306 component are in phase with precession index maxima. The precession cycles in the ln(Fe/Ca)
1307 record appear particularly strong between ~0.9 and 0.6 Ma.
1308 e), f) and g) present the same statistical analyses as in a), b) and c) respectively but for the
1309 PC1 SST record. For e) dashed white lines indicate the variability at the precession, obliquity
1310 and eccentricity periods. The three statistical analyses indicate significant variability at the
1311 100 and 41 kyr periods but not significant power for the 400 kyr and 23 kyr (precession)
1312 periods.

1313

1314 **Extended Data Figure 6: SST proxies reconstruction for core MD96-2048 over the last**
1315 **2.14 Ma.** a) Reconstruction of SST using two different methods: Mg/Ca reconstruction based
1316 on Caley et al.¹⁵ data and new data. Mg/Ca ratios were converted into temperature values
1317 applying the equation established by Anand et al.⁴⁰. Foraminifera transfer function
1318 reconstruction using the modern analogue technique. Error bars represent the error on the
1319 calibrations⁴⁰ (Extended data Fig. 7). b) Empirical Orthogonal Function (EOF) analysis⁴⁷ on
1320 the two SST records over the last 2.14 Ma. The Principal Component (PC1) contains 74 % of
1321 the total variance over the last 2.14 Ma. Correlation between SST proxies and PC1 over the
1322 last 2.14 Ma is $R = 0.71$.

1323

1324 **Extended Data Figure 7: Foraminifera transfer function used for core MD96-2048.** a)
1325 Location of the modern database composed of 367 core tops from the south Indian Ocean⁴⁵
1326 with present day SST from WOA 2009²⁹. b) Test for the modern database composed of 367
1327 core tops from the south Indian Ocean⁴⁵ yielding to a precision of 0.8°C for the annual SST
1328 reconstructions. Modern hydrological parameters were obtained from the WOA (1998)
1329 database using the tool developed by Schäfer-Neth in the MARGO project
1330 (<http://www.geo.uni-bremen.de/geomod/Sonst/Staff/csn/woasample.html>).

1331

1332 **Extended Data Table 1: Fossil finds, their location, and the associated ages.** We consider
1333 the ages in bold as the best estimate. The different dating methods did not yield any
1334 agreement regarding the age of Kromdraai B and Sterkfontein Member 5 “Oldowan Infill”.
1335 Therefore, no estimate are highlighted in bold and the stratigraphic ranges are not showed in
1336 Fig. 3. We favor U-Pb dates and cosmogenic burial of quartz dates rather than biochronology
1337 or ESR (although dates are generally not inconsistent with the other methods)¹⁴⁵. **P. robustus*
1338 fossils were not found at GD1 and GD2 but nearby ex situ. Given the close age between GD1

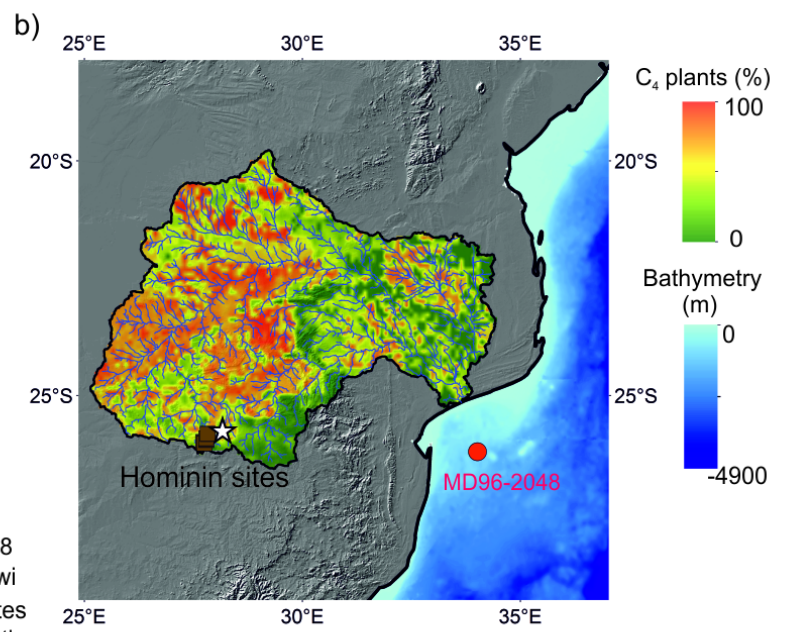
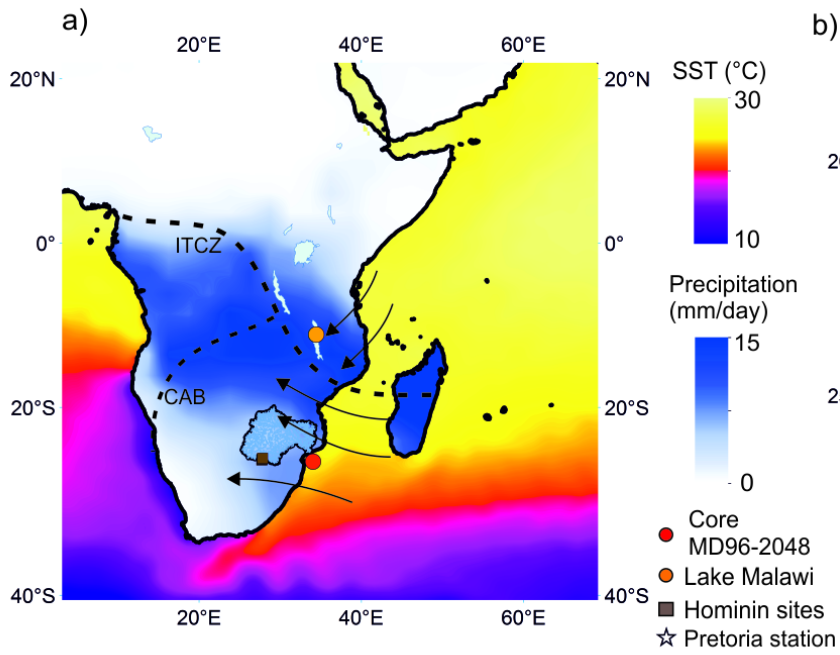
1339 and GD2 and the limited extent of outcrops, it was suggested that the ex situ hominin
1340 specimens from Gondolin should be dated around 1.78 Ma.

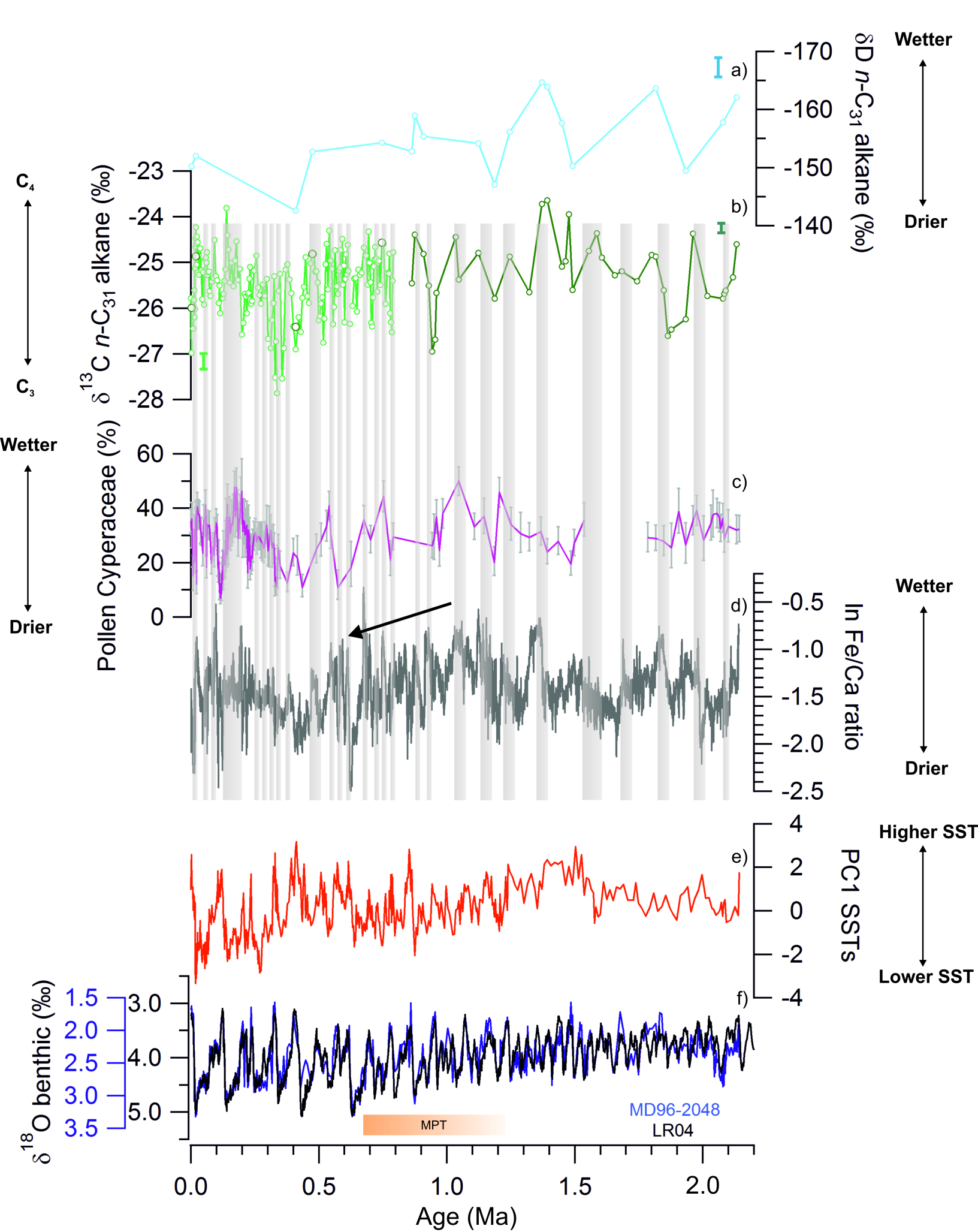
1341

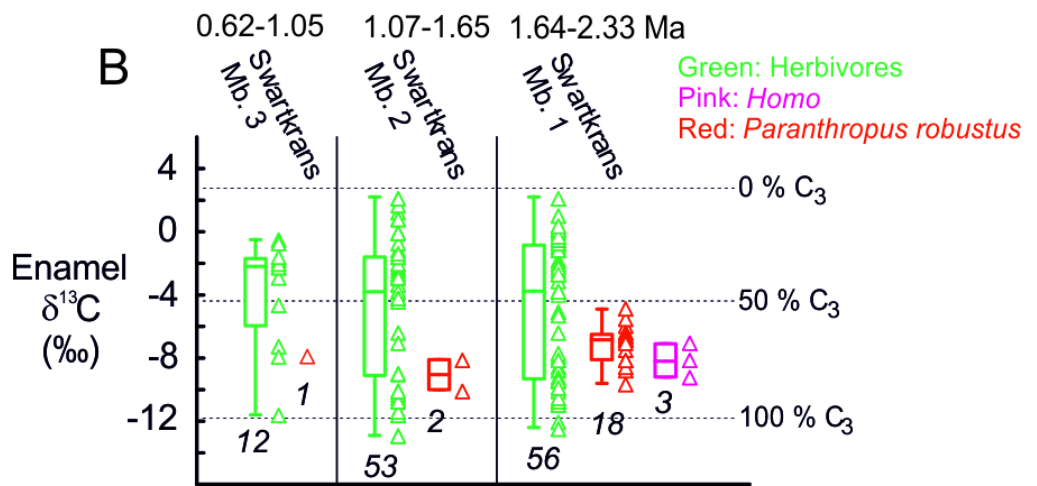
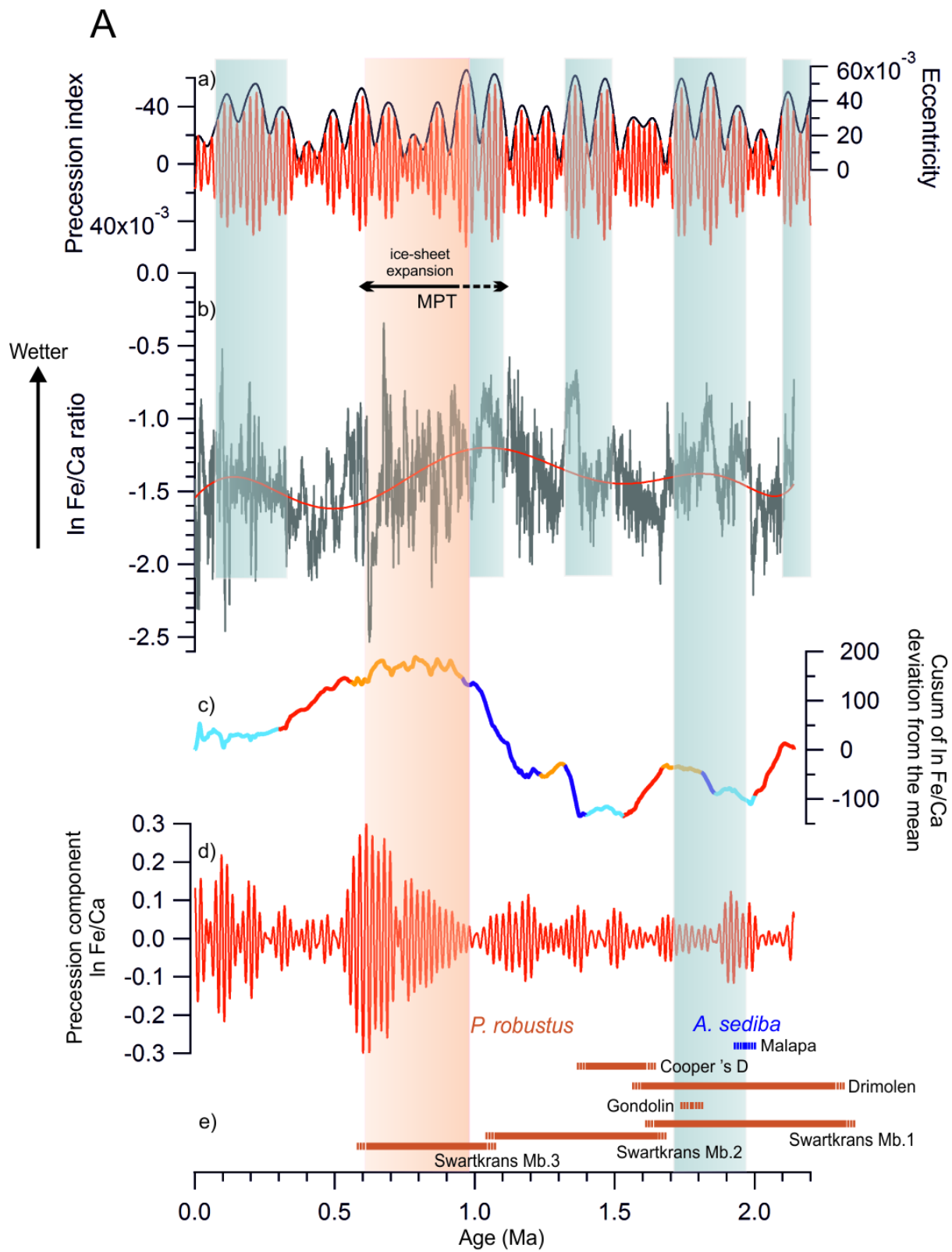
1342 **Extended Data Table 2: $\delta^{13}\text{C}$ enamel of hominin and contemporaneous herbivores and**
1343 **associated statistical parameters for different sites in the Limpopo catchment.**

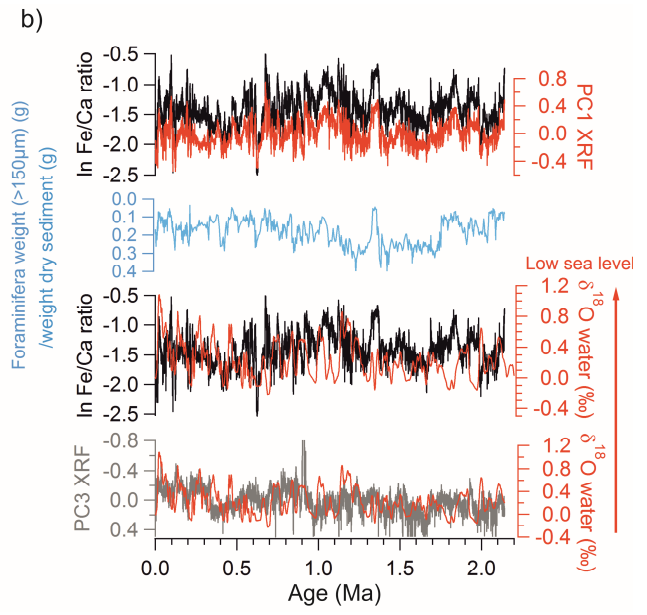
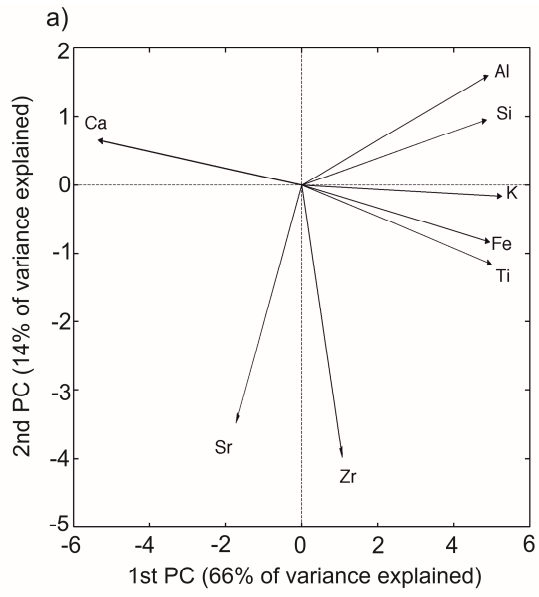
1344

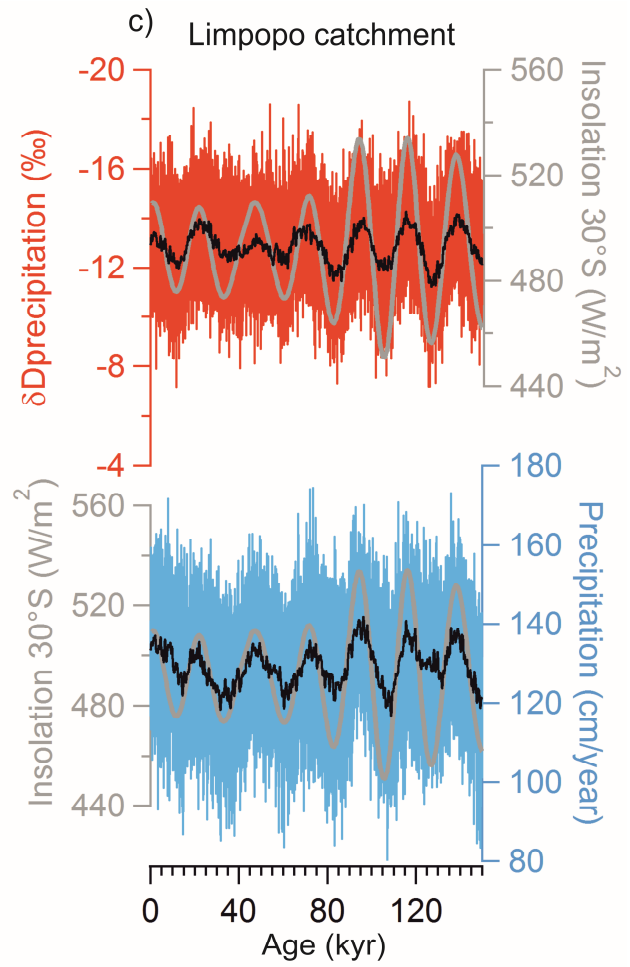
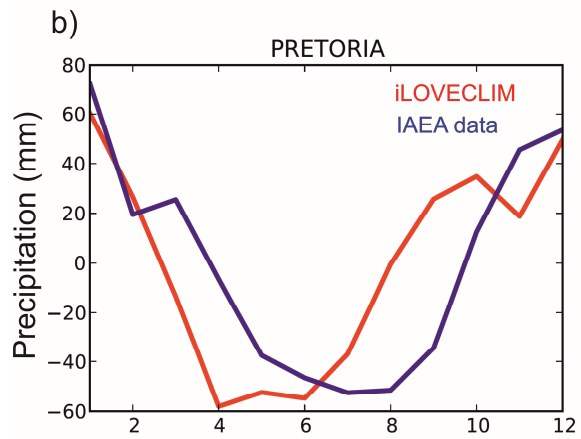
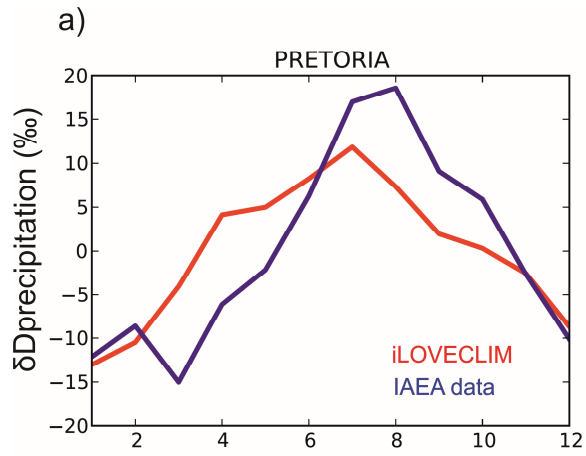
1345

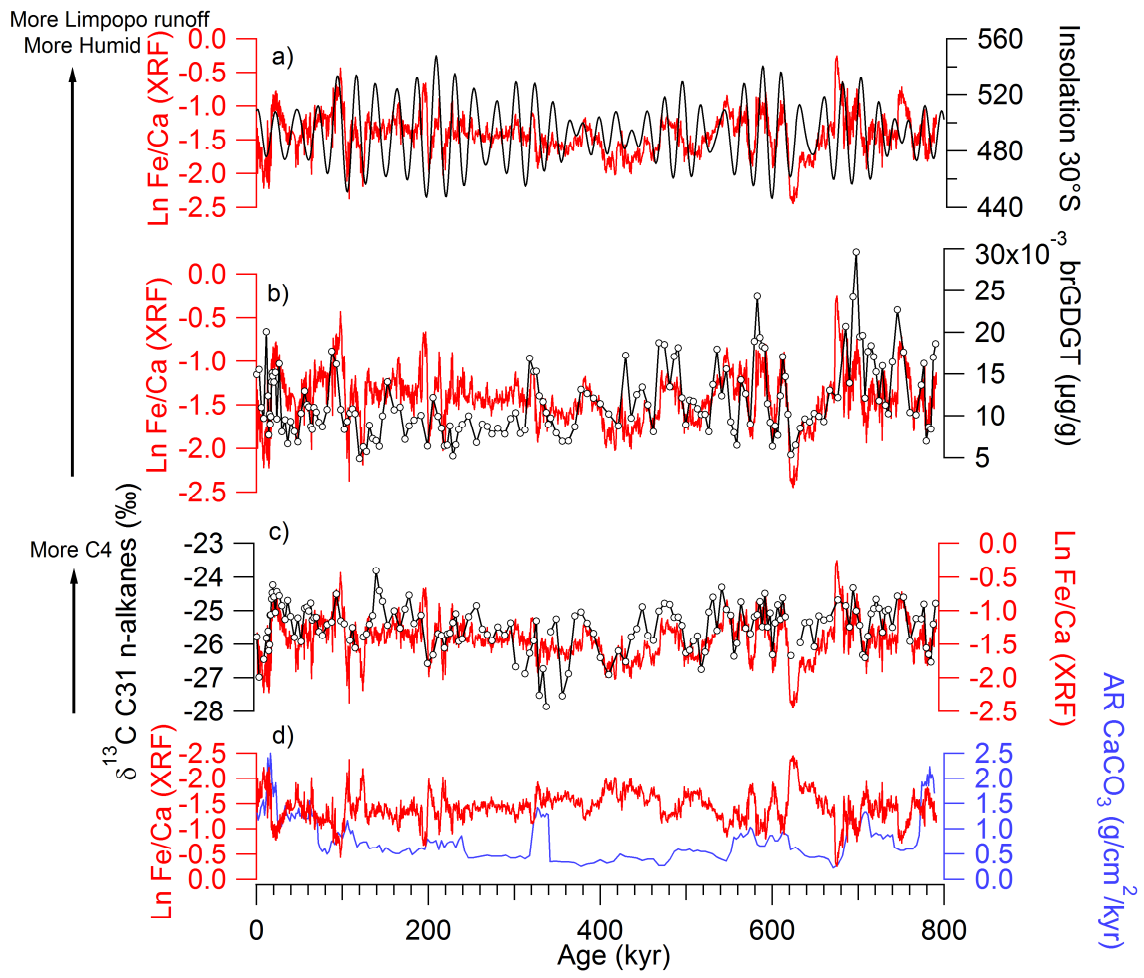


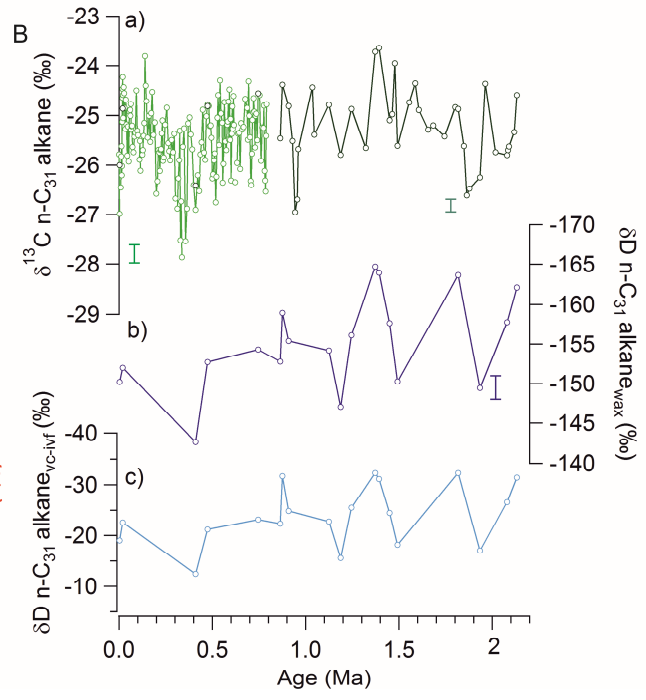
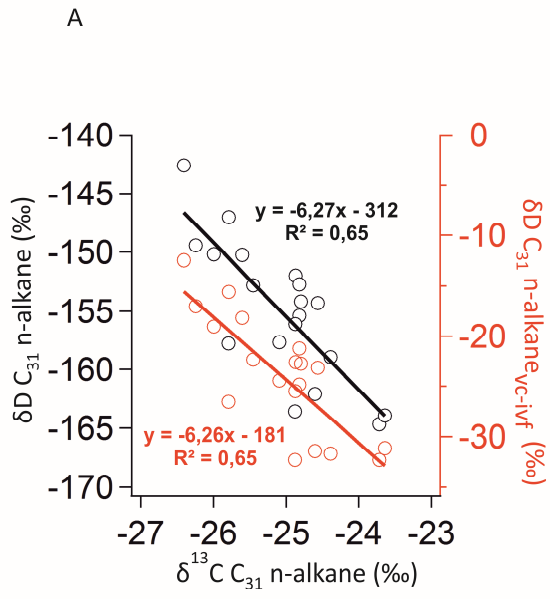


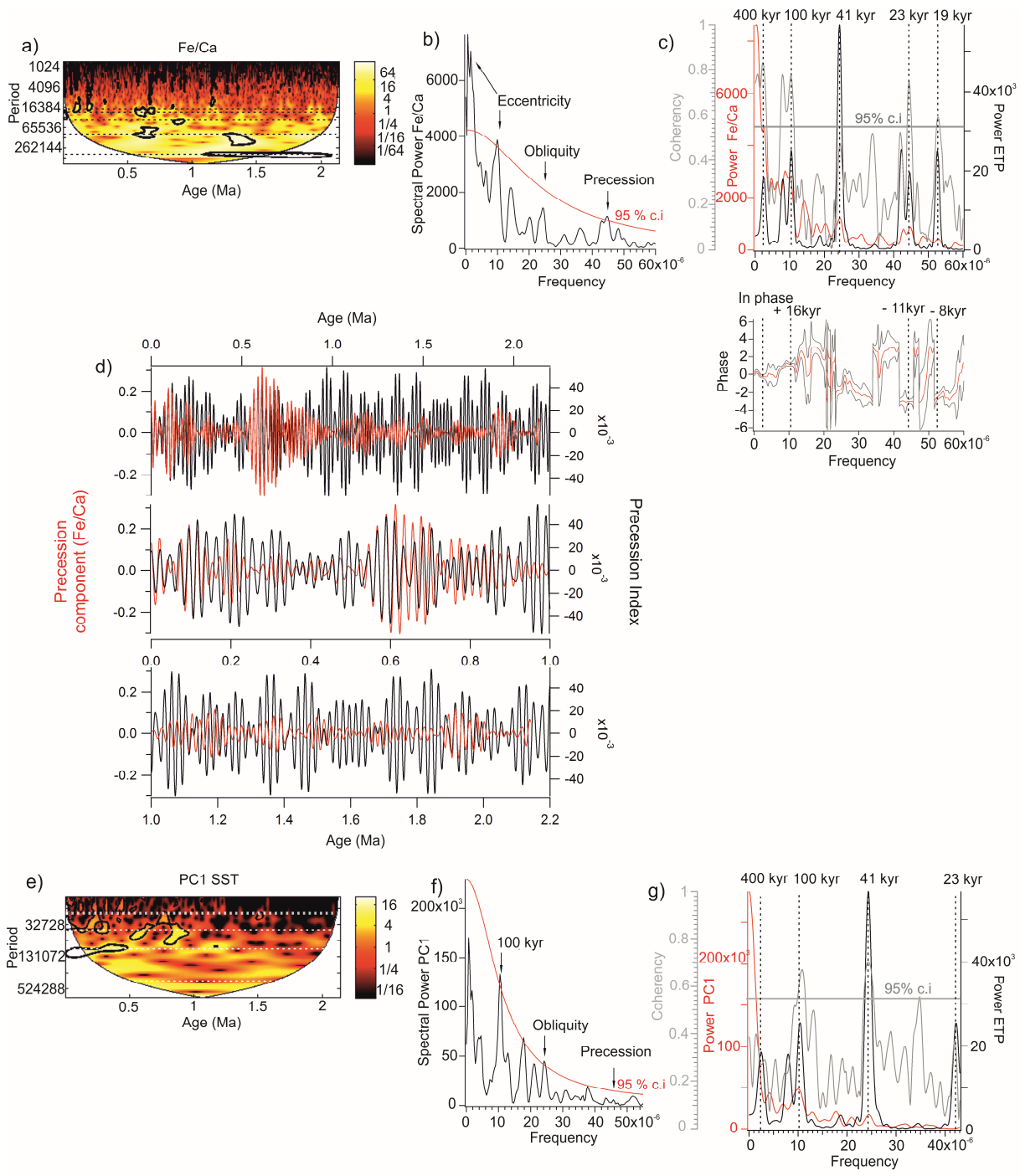


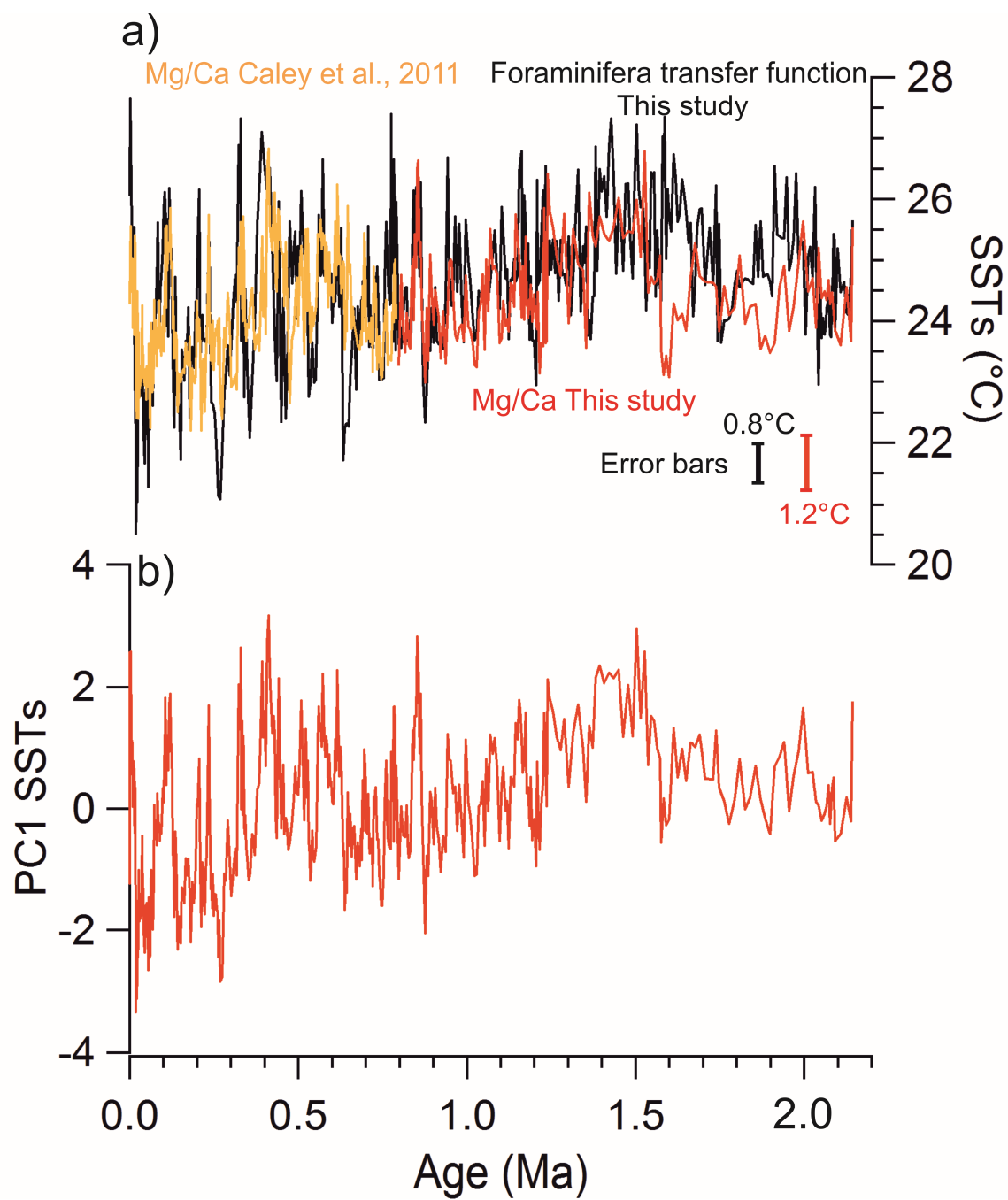


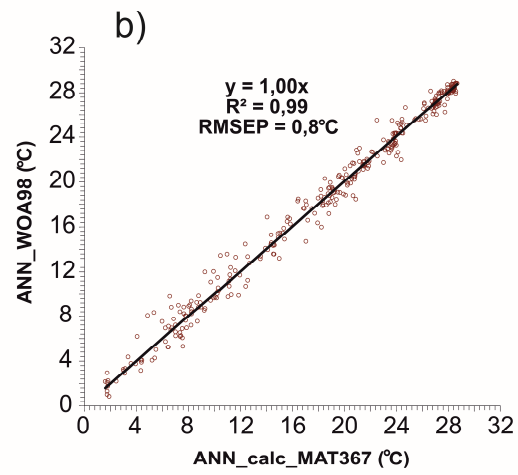
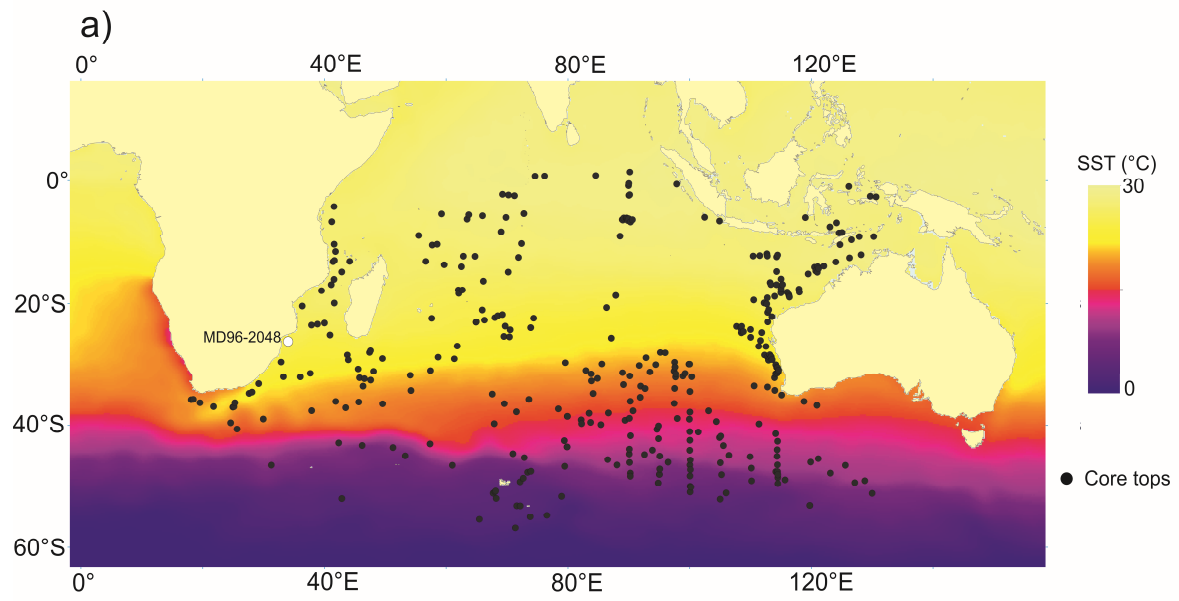












Site/area	Taxon	Stratigraphic unit	Methods	References	Estimated age of fossils
Malapa	<i>Australopithecus sediba</i>		Biochronology U-Pb dating of flowstones: basal flowstone 1 at 2.026 ± 0.021 Ma; capping flowstone 2 at 2.048 ± 0.140 Ma Paleomagnetism : reversed polarity of flowstone 2, normal polarity of fossiliferous sediments Synthesis of flowstone dating and paleomagnetism, 1.977 ± 0.002 Ma	Dirks et al. (137) Pickering et al. (138) Pickering et al. (138) Pickering et al. (138)	From 1.95 Ma to 1.78 Ma From 2.188 Ma to 1.908 Ma Older than 1.95 Ma From 1.979 to 1.975 Ma
Cooper's D	<i>Paranthropus robustus</i>		Biochronology U-Pb dating of flowstones: basal flowstone CDD1 at 1.526 ± 0.088 Ma; younger flowstone CDD3, intercalated within fossiliferous sequence, at ca. 1.4 Ma (unprecise dating from 1.617 Ma to 1.413 Ma)	Berger et al. (139) de Ruiter et al. (140)	From 1.9 Ma to 1.6 Ma From 1.615 Ma to ca. 1.4 Ma (upper facies A and C) and younger than 1.4 Ma (lower facies A and C)
Drimolen	<i>P. robustus</i>	Main Quarry Site	Biochronology Biochronology	Keyser et al. (141) Adams et al. (142)	From 2.0 Ma to 1.5 Ma From 2.3 Ma to 1.6 Ma
Kromdraai B	<i>P. robustus</i>		Paleomagnetism of flowstone above Mb. 3, reverse polarity, older than normal Olduvai event (between 1.95 Ma and 1.78 Ma) Alternative interpretation of paleomagnetic data from Thackeray et al. (2002) Biochronology (including hominins) and paleomagnetism	Thackeray et al. (143) Herries et al. (144); Herries & Adams (145) Braga et al. (146)	Older than 1.95 Ma From 1.78 Ma to 1.65 Ma Older than 2.18 Ma
Gondolin	<i>P. robustus</i>	GD2*	Biochronology and paleomagnetism (Olduvai normal polarity event of fossiliferous sediments)	Herries et al. (147)	Slightly older than 1.78 Ma
	<i>P. robustus</i>	GD1*	Biochronology and paleomagnetism (end of Olduvai normal polarity event in basal flowstone)	Adams et al. (148)	Slightly younger than 1.78 Ma
Sterkfontein	<i>P. robustus</i>	Mb. 5B "Oldowan infill"	Biochronology and lithic typology ESR on bovid teeth (seven dates): 1.328 ± 0.087 Ma; 1.315 ± 0.295 Ma; 1.185 ± 0.96 Ma; 1.265 ± 0.125 Ma; 1.620 ± 0.626 Ma; 0.965 ± 0.147 Ma; 1.24 ± 0.28 Ma; weighed mean = 1.32 ± 0.08 Ma Synthesis of ESR, U-Pb dating, paleomagnetism	Kuman & Clarke (106) Curnoe (149) reinterpreted in Herries & Shaw (150) Herries & Shaws (150)	From 2.0 Ma to 1.7 Ma From 1.40 Ma to 1.24 Ma From ca. 1.4 Ma to 1.2 Ma
		Mb. 5B "Oldowan infill"	ESR on teeth from 0.965 ± 0.147 Ma to 1.328 ± 0.087 Ma ; weighted mean LU-ESR (excluding one tooth with large internal errors) = 1.223 ± 0.155 Ma	Curnoe (149) reinterpreted in Herries et al. (144)	from 1.415 Ma to 1.241 Ma (maximal); 1.112 Ma to 0.818 Ma (minimal); from 1.378 Ma to 1.223 Ma (weighed mean)
		Mb. 5B "Oldowan infill"	Cosmogenic burial (²⁶ Al/ ⁹ Be) dating of a quartz manuport 2.18 ± 0.21 Ma	Granger et al. (151)	From 2.39 Ma to 1.97 Ma
		Mb. 5B "Oldowan infill"	Synthesis of paleomagnetism, U-Pb dating, and ESR	Herries & Adams (145)	From 1.8 Ma to 1.5 Ma
		Mb. 5B "Oldowan infill"	Synthesis of biochronology and ESR	Herries et al. (144)	From 1.38 Ma to 1.07 Ma
Swartkrans	<i>P. robustus</i>	Mb. 1	Cosmogenic burial (²⁶ Al/ ⁹ Be) dating on quartz 2.19 ± 0.08 Ma	Gibbon et al. (152)	From 2.27 Ma to 2.11 Ma
		Mb. 1	Cosmogenic burial (²⁶ Al/ ⁹ Be) dating on quartz 1.80 ± 0.09 Ma	Gibbon et al. (152)	From 1.89 Ma to 1.71 Ma
		Mb. 1 Hanging Remnant	Synthesis of U-Pb dating and ESR	Herries & Adams (145)	From 2.0 Ma to 1.8 Ma
		Mb. 1 Hanging Remnant	ESR 2.02 ± 0.36 Ma; 2.07 ± 0.37 Ma; 1.68 ± 0.28 Ma; weighed mean = 1.96 Ma-1.70 Ma	Curnoe et al. (153) reinterpreted in Herries & Adams (145)	From 1.96 Ma to 1.70 Ma
		Mb. 1 Hanging Remnant	ESR LU 1.39 ± 0.18 Ma	Herries et al. (144)	From 1.57 Ma to 1.21 Ma
		Mb. 1 Hanging Remnant	ESR LU 1.92 ± 0.34 Ma	Herries et al. (144)	From 2.26 Ma to 1.58 Ma
		Mb. 1 Hanging Remnant	ESR LU 1.21 ± 0.22 Ma	Herries et al. (144)	From 1.43 Ma to 0.99 Ma
		Mb. 1 Lower Bank	U-Pb dating	Pickering et al. (154)	From 2.3 to 1.6 Ma
		Mb. 1	U-Pb dating on tooth 1.83 ± 1.38 Ma	Balter et al. (155) Vrba (156, 157); Churcher & Watson (158)	From 3.21 to 0.45 Ma ca. 1.7 Ma
		Mb. 1	Biochronology	Churcher & Watson (158)	ca. 1.7 Ma
		Mb. 1	U-Pb dating of basal flowstone 2.249 ± 0.077 Ma; top flowstone 1.706 ± 0.069 Ma ; closer to 2.0 Ma-1.8 Ma	Pickering et al. (154)	Maximal range from 2.326 Ma to 1.637 Ma; minimal range from 2.172 Ma to 1.775 Ma
Swartkrans	<i>P. robustus</i>	Mb. 2	U-Pb dating on tooth 1.36 ± 0.29 Ma	Balter et al. (155) Vrba (156, 157); Churcher & Watson (158)	From 1.65 Ma to 1.07 Ma ca. 1.5 Ma
		Mb. 2	Biochronology	Churcher & Watson (158)	ca. 1.5 Ma
		Mb. 2	Relative position to Mb. 1 dated by U-Pb	Pickering et al. (154)	Younger than ca. 1.7 Ma
Swartkrans	<i>P. robustus</i>	Mb. 3	Synthesis of U-Pb and ESR dating	Herries & Adams (145)	From 1.3 Ma to 0.6 Ma
		Mb. 3	Cosmogenic burial on quartz 0.96 ± 0.09 Ma	Gibbon et al. (152)	From 1.05 Ma to 0.87 Ma
		Mb. 3	ESR 0.65 ± 0.15 Ma	Cited in Herries and Adams (145)	From 0.8 Ma to 0.5 Ma
		Mb. 3	ESR 1.25 ± 0.09 Ma	Cited in Herries and Adams (145)	From 1.34 Ma to 1.16 Ma
		Mb. 3	U-Pb dating on tooth 0.83 ± 0.21 Ma	Balter et al. (155) Vrba (156, 157); Churcher & Watson (158)	From 1.04 Ma to 0.62 Ma ca. 1.0 Ma
		Mb. 3	Biochronology	Churcher & Watson (158)	ca. 1.0 Ma
		Mb. 3	ESR LU on two bovid teeth (four dates): 0.71 ± 0.90 Ma and 0.80 ± 0.15 Ma; 0.65 ± 0.15 Ma and 0.70 ± 0.11 Ma; mean = 0.72 ± 0.13 Ma	Blackwell (159)	From 0.85 Ma to 0.59 Ma
		Mb. 3	Synthesis of biochronology and U-Pb	Herries et al. (144)	From 1.04 Ma to 0.62 Ma

Group	n	$\delta^{13}\text{C}$ (‰)		mode(s) (2 ‰ interval)	SD	min max range			References
		mean	median			min	max	range	
Cooper' D herbivores	45	-5,0	-4,7	int. 1: -12 to -10 ‰ ; int. 2: -2 to 0 ‰	3,9	-11,5	2,5	14,0	Steininger (101)
Gondolin GD2 herbivores	21	-2,9	1,0	int. 1: -10 to -8 ‰ ; int. 2: 0 to 2 ‰	5,3	-11,1	3,5	14,6	Adams (102) Lee-Thorp et al. (99); Sponheimer et al. (83);
Swartkrans Mb. 1 herbivores	56	-4,8	-3,8	int. 1: -10 to -8 ‰ ; int. 2: -4 to 0 ‰	4,2	-12,4	2,2	14,6	Steininger (160) Lee-Thorp et al. (99); Sponheimer et al. (84,
Swartkrans Mb. 1 <i>Paranthropus</i>	18	-7,2	-6,9	int.: -8 to -6 ‰	1,2	-9,6	-4,9	4,7	83)
Swartkrans Mb. 1 <i>Homo</i>	3	-8,2	-8,2	int.: -10 to -8 ‰ int. 1: -12 to -10 ‰ ; int. 2: -4 to -2 ‰	0,9	-9,2	-7,1	2,1	Lee-Thorp et al. (100) Lee-Thorp et al. (99, 100); Steininger (160)
Swartkrans Mb. 2 herbivores	53	-4,8	-3,8		4,4	-12,9	2,2	15,1	
Swartkrans Mb. 2 <i>Paranthropus</i>	2	-9,1	-9,1			-10,0	-8,1	1,9	Lee-Thorp et al. (99)
Swartkrans Mb. 3 herbivores	12	-3,8	-2,2	int.: -4 to 0 ‰	3,3	-11,6	-0,5	11,1	Steininger (160)
Swartkrans Mb. 3 <i>Paranthropus</i>	1	-7,9	-7,9			-7,9	-7,9		Lee-Thorp et al. (99)